JPRS L/9142

16 June 1980

USSR Report

PHYSICS AND MATHEMATICS

(FOUO 5/80)

FBIS FOREIGN BROADCAST INFORMATION SERVICE

NOTE

JPRS publications contain information primarily from foreign newspapers, periodicals and books, but also from news agency transmissions and broadcasts. Materials from foreign-language sources are translated; those from English-language sources are transcribed or reprinted, with the original phrasing and other characteristics retained.

Headlines, editorial reports, and material enclosed in brackets [] are supplied by JPRS. Processing indicators such as [Text] or [Excerpt] in the first line of each item, or following the last line of a brief, indicate how the original information was processed. Where no processing indicator is given, the information was summarized or extracted.

Unfamiliar names rendered phonetically or transliterated are enclosed in parentheses. Words or names preceded by a question mark and enclosed in parentheses were not clear in the original but have been supplied as appropriate in context. Other unattributed parenthetical notes within the body of an item originate with the source. Times within items are as given by source.

The contents of this publication in no way represent the policies, views or attitudes of the U.S. Government.

For further information on report content call (703) 351-2938 (economic); 3468 (political, sociological, military); 2726 (life sciences); 2725 (physical sciences).

APPROVED FOR RELEASE: 2007/02/08: CIA-RDP82-00850R000200090028-0

JPRS L/9142

16 June 1980

USSR REPORT

PHYSICS AND MATHEMATICS

(FOUO 5/80)

CONTENTS

ACOUSTICS

UDC 534.2

DIFFRACTION OF SOUND PULSES BY ELASTIC BODIES

Moscow DIFRAKTSIYA AKUSTICHESKIKH IMPUL'SOV NA UPRUGIKH TELAKH in Russian 1979 signed to press 10 July 79 pp 2, 3-4, 238-239

[Annotation, foreword, and table of contents from a book by Yaan Aleksandrovich Metsaveer, Naum Davidovich Veksler, and Anatoliy Svyatovslavovich Stulov, Nauka, 1400 copies, 239 pages]

[Text] This monograph describes methods for calculating acoustic echo signals from deformable bodies and the use of these signals for determining the geometrical and physical parameters of the scattering bodies. The echo signals investigated come from thin shells and solid bodies of spherical, cylindrical, and arbitrary shape. Stress waves in thin elastic shells are investigated in the framework of the equations of motion corresponding to Timoshenko's linear shell theory, while stress waves in solids are studied by assuming the equations of linear elasticity theory. The medium surrounding the body is assumed to be infinite, and its motion is described by the equations of an ideal compressible fluid. Acoustic echo signals are calculated primarily in the form of individual echo pulses, but algorithms primarily in the form of individual echo pulses, but algorithms are proposed both for calculating the principal parts of the quasi-steady state approximations of echo signals and for finding their wavefront regions. Numerical results are given. Algorithms for determining the parameters of thin shells from acoustic echo signals are described.

This monograph is intended for the use of a broad range of scientists, students, and graduate students specializing in the fields of hydroacoustics and the mechanics of deformable solids. Figures 44; references 280: 146 Russian, 134 Western.

FOREWORD

The theory of the diffraction of acoustic waves by elastic bodies is considered in this book. The authors do not go beyond the linear formulation of the problem. The basic working method involves integral transforms, and the basic goal is the investigation of unsteady wave fields in a fluid. Systematic study is given to reflected and emitted, peripheral and creeping

pulses, and also to pulses passing through a liquid filler that are produced by an acoustic pressure pulse incident on an elastic body. The results of an analysis of these pulses are used to develop algorithms for determining the parameters of an elastic body from an acoustic echo signal.

Two-dimensional diffraction problems are considered in the monograph. Problem formulation is discussed in the first chapter. The second chapter considers the problems of diffraction by bodies of spherical shape: a thin elastic shell with a fluid filler and a hollow shell of revolution whose meridian is close to a circle. The third chapter discusses the problems of diffraction by bodies having the shape of a circular cylinder: a thin elastic shell with a fluid filler, a hollow cylindrical shell, and a solid elastic cylinder. Diffraction by bodies of arbitrary shape is considered in the fourth chapter. The theory of peripheral waves on a noncircular cylinder is generalized, a way of solving the problem of diffraction by the Bubnov-Galerkin method is proposed, the reflection of sound waves from a solid elastic body is investigated, and a method of solving the nonstationary problem of diffraction by elastic bodies with the use of integral boundary equations is described. An algorithm for determining the parameters of a shell from a recorded acoustic echo signal is proposed in the fifth chapter.

The book discusses the results obtained by the authors in their research of hydroacoustics carried out at the Institute of Cybernetics of the Academy of Sciences of the Estonian SSR.

N. D. Veksler wrote sections 1-3, 5-7, 9, 11, and 15; Ya. A. Metsaveer wrote sections 4, 8, 10, 13, 14, 17, 18, along with Sec. 5.2 and the problems referring to pulses passing through a filler in Sec. 5; A. S. Stulov wrote Secs. 12 and 16; Yu. P. Pikk helped to obtain the results given in Secs. 4 and 8; M. E. Kutser discussed the problems referring to pulses passing through a filler in Sec. 9; V. M. Korsunskiy helped to obtain the results in Sec. 6.5.

The authors are grateful to Profs. N. A. Alumyae, U. K. Nigul, and L. Ya. Aynola for useful discussions that improved the manuscript.

TABLE OF CONTENTS

9370
CSO: 1862

CRYSTALS AND SEMICONDUCTORS

CRYSTALLIZATION PHYSICS

Kalinin FIZIKA KRISTALLIZATSII: MEZHVUZOVSKIY TEMATICHESKIY SBORNIK (Crystallization Physics: Thematic Anthology for Higher Schools) in Russian 1979 signed to press 20 Apr 79 pp 2, 143-144

[Annotation and table of contents from book edited by T. V. Mikushin, 300 copies, 144 pages]

[Text] The thematic collection for higher schools, "Fizika kristallizatsii" chiefly deals with subjects relating to the research into the mechanism of crystal growth, the kinetics of growth and dissolution, the effect of growing conditions on morphology, and crystal defects and impurities. Clearly, the views of crystal growth expressed by the authors of the papers published in this collection may not coincide.

The Editorial Board strives to enlist participation in this collection by experts in the field of industrial crystallogeny. Papers on crystal properties are not accepted for this collection unless they deal with a direct relationship between properties and growth. In this respect Spedding's comment is pertinent: "If some property has to be measured, 80 percent of the effort and ingenuity is usually expended on either obtaining the metal or alloy in a highly pure form and on growing a single crystal of corresponding purity or 'characterizing' the obtained crystal in order to know exactly what is represented by the material which is to be used for the measurements. And only 20 percent of all effort is usually expended on the measurement of the investigated property itself."

The Editorial Board regards as highly desirable participation in this collection by the leading experts in the genesis of natural crystals, thus emphasizing the universality of the laws governing the commercial synthesis of crystals and the growth of crystals in nature.

The next issue in this series will be devoted to morphological aspects relating to the formation and growth of crystals.

Editorial Board: Candidate of Engineering Sciences Yu. M. Smirnov (Coordinating Editor), Doctor of Physical-Mathematical Sciences Professor L. M. Shcherbakov, Doctor of Physical-Mathematical Sciences D. D. Mishin, Doctor

of Engineering Sciences V. N. Romanenko, Candidate of Geological-Mineralogical Sciences B. N. Litvin, Junior Scientific Co-Worker V. A. Shmidt (Technical Secretary).

Contents

Contents Page

1386
CSO: 1862

FLUID DYNAMICS

GAS AND WAVE DYNAMICS

Moscow GAZOVAYA I VOLNOVAYA DINAMIKA, VYPUSK 2 [No 2] in Russian 1979 signed to press 9 Jan 79 pp 2, 199-200

[Annotation and table of contents from book edited by Khalil Akhmedovich Rakhmatulin, Izdatel'stvo Moskovskogo Universiteta, 200 pages]

[Text] This collection contains articles reflecting both traditional and new trends under development in the department of gas and wave dynamics of the mechanics-mathematics faculty. A major part of the studies presented is devoted to problems of gas dynamics and the dynamics of a deformable solid.

This collection is intended for specialists in the field of the mechanics of a continuous medium and for graduate students and students.

CONTENTS Page

8831
CSO: 1862

LASERS AND MASERS

UDC 621.373.826.038.823

CONCERNING SELF-OSCILLATORY INSTABILITY IN FAST-FLOW LASERS WITH UNSTABLE RESONATORS

Moscow KVANTOVAYA ELEKTRONIKA in Russian Vol 7, No 2(92), Feb 80
pp 237-243 manuscript received 3 Apr 79

[Article by V. V. Likhanskiy and A. P. Napartovich, Institute of Atomic Energy imeni I. V. Kurchatov, Moscow]

[Text] 1. At the present time, unstable resonators are extensively used in fast-flow lasers. In a theoretical paper [Ref. 1] it has been shown by the example of the simplest model of an active medium that a self-oscillatory mode of operation may arise in such systems. Experiments [Ref. 2, 3] have shown modulation of the output emission of a CO_2 laser with characteristic frequencies corresponding to the time of flight of the active medium through the resonator region. In Ref. 4, by a method analogous to Ref. 1, a condition was derived for the distribution of intensity through the resonator of a laser with steady-state pumping in the volume that gives rise to instability. It was shown that pumping of the active medium in the resonator region may lead to stabilization of the steady state.

It was numerically shown in Ref. 5 that exchange of excitations between molecules of N_2 and CO_2 stabilizes the steady state, while accounting for the finiteness of time of emission output from the laser cavity for ordinary conditions essentially changes nothing. In Ref. 6 in the model of the active medium of a CO_2 laser with approximate consideration of exchange $N_2 \rightleftharpoons CO_2$, the boundary of development of self-oscillatory instability was numerically found. In particular it was found that when $k_{in}/k_{th}>2$, instability arises when $\tau_{tf}x_C/(\tau_{NC}x_N) \gtrsim 8$. Here k_{in} is the gain at the input to the resonator zone; k_{th} is the threshold gain; τ_{tf} is the time of flight of the medium from the inlet to the axis of the resonator; $\tau_{NC}^{-1} = K_0 N x_N$; K_0 is the rate constant of exchange of vibrational excitation between N_2 and the upper laser level of CO_2; N is the total gas density; x_C, x_N are the molar percentages of CO_2 and N_2 in the laser mixture.

The influence that the enumerated factors (exchange between N_2, CO_2 and pumping in the resonator zone) have on lasing stability in a fast-flow

laser has been studied numerically heretofore. Analytical criteria are derived below for laser working stability as a function of the parameters of the working medium and the pumping parameters.

2. Our examination will be carried out within the framework of the model of the working medium of a CO_2 laser presented in Ref. 6. Let us briefly outline the derivation of this model.

In the approximation of a small degree of vibrational excitation [Ref. 7] and assuming rapid relaxation from the lower lasing level of CO_2, the kinetic equations will take the form

$$\frac{\partial n_C}{\partial t} - v\frac{\partial n_C}{\partial x} = -K_0 N x_N\left(n_C - \frac{x_C}{x_N}n_N\right) - \frac{\sigma I n_C}{\hbar\omega} - \frac{n_C}{\tau_p} + Q_C; \quad (1)$$

$$\frac{\partial n_N}{\partial t} - v\frac{\partial n_N}{\partial x} = -K_0 N x_C\left(n_N - \frac{x_N}{x_C}n_C\right) + Q_N, \quad (2)$$

where n_C is the population on level (001) of CO_2; n_N is the concentration of vibrationally excited nitrogen; v is the velocity of the gas flow; σ is the cross section of stimulated emission; $\hbar\omega$ is the transition energy; I is the intensity of laser emission; τ_p is the time of relaxation of level (001) of CO_2 as calculated for mixtures according to known rules (the relaxation of nitrogen is disregarded); Q_C, Q_N are the rates of excitation of CO_2 and N_2 by an external source (discharge). When $x_C \ll x_N$ equations (1), (2) are simplified since the degree of excitation of CO_2 quasi-steadily follows the change of concentration n_N. The transition region is small compared with the dimension of the resonator along the flow, if $\tau_{tf} \gg 1/(K_0 N x_N), (\sigma I/\omega)^{-1}$. This requirement actually coincides with the condition of high efficiency of energy extraction in the resonator when $x_C \ll x_N$. In this case

$$n_C = (n_N x_C/x_N + Q_C\tau_{NC})/(1+\tau_{NC}\sigma I/\hbar\omega + \tau_{NC}/\tau_p). \quad (3)$$

The equation for n_N is obtained by substituting (3) in (2). In the absence of pumping and when relaxation plays a small part ($\tau_{NC} \ll \tau_p$) the equation for n_N takes the form shown in Ref. 1:

$$\frac{\partial n_N}{\partial t} - v\frac{\partial n_N}{\partial x} = -\frac{x_C n_N}{x_N \tau_{NC}}\frac{\sigma I \tau_{NC}}{\hbar\omega(1+\sigma I\tau_{NC}/\hbar\omega)}. \quad (4)$$

Let us note that accounting for filling of the lower laser level during lasing within the framework of the model of Ref. 7 when $x_C \ll x_N$ is also readily taken care of. In formula (4) in this case we must replace $1+\sigma/\tau_{NC}/\hbar\omega$ by $1+\sigma/\tau_{NC}/\hbar\omega+\sigma/\tau_{1eff}/\hbar\omega$, where $\tau_{eff} = 2\tau_1 \exp(-960/T_1)$, T_1 is the temperature of the deformation mode, τ_1 is the relaxation time of the deformation mode of CO_2.

Hereafter, to avoid long formulas in our presentation, we will make separate examinations of stabilization of self-oscillatory instability [Ref. 1] by external pumping and by N_2-CO_2 exchange.

3. Before going on to solve the formulated problem, let us consider an auxiliary resonator model that is also of independent interest. We will assume that intensity is uniform over the cross section of the resonator, and that its value is determined by the lasing condition $k_y(0) = d(M-1)/2L$ set up on the resonator axis. Here $d = 1$ for cylindrical resonator mirrors, and $d = 2$ for spherical laser mirrors; L is the length of the active medium along the resonator axis; M is the magnification ratio. This model should reasonably describe an unstable resonator with field rotation as proposed by Anan'yev [Ref. 8]. It easily gives steady-state solutions and can be used to construct a linear theory of stability.

First let us consider the part played by pumping in stability of the lasing mode. We disregard saturation of exchange ($\tau_{NC} \to 0$). Then the equation for n_C takes the form

$$\frac{\partial n_C}{\partial t} - v\frac{\partial n_C}{\partial x} = -\frac{x_C}{x_N} n_C\left(\frac{\sigma I}{\hbar\omega} + \frac{1}{\tau_p}\right) + \frac{x_C}{x_N} Q_N. \qquad (5)$$

Let us convert to dimensionless quantities $k = 2L\sigma n_C/(M-1)$, $\tau = tv/l$, $\xi = x/l$, $u = \sigma I x_C l/(\hbar\omega x_N v)$, $\eta = \tau_p v/l$, $q = (x_C/x_N)2Ll\sigma Q_N/(M-1)$, where l is the distance from the resonator input to its axis. Then equation (5) takes the form

$$\partial k/\partial\tau - \partial k/\partial\xi = -k(u+\eta^{-1}) + q. \qquad (6)$$

This equation must be supplemented by two conditions

$$k(0) = d, \quad k(1) = k_0, \qquad (7)$$

where $k_0 = 2Lk_{in}/(M-1)$, defining $k(\xi,\tau)$ and $u(\tau)$.

Without writing out the steady-state solution of problem (6), (7), let us go on to the linear analysis of its stability. We represent the functions k and u in the form

$$u = u_{cr} + \tilde{u}\exp(\gamma\tau), \quad k = k_{cr}(\xi) + \tilde{k}(\xi)\exp(\gamma\tau). \qquad (8)$$

[The subscript CT indicates "steady-state"]. Here $\tilde{k}$ satisfies the equation

$$\partial\tilde{k}/\partial\xi = (u_{cr} + \eta^{-1} + \gamma)\tilde{k} + k_{cr}\tilde{u} \qquad (9)$$

and the conditions

$$\tilde{k}(0) = \tilde{k}(1) = 0. \qquad (10)$$

Solving (9), (10), we find the equation for eigenvalues γ

$$1 - e^{-\gamma} = \int_0^1 q\, e^{-(u_{cr}\pm\eta^{-1})\xi}(e^{-\gamma\xi} - e^{-\gamma})d\xi. \qquad (11)$$

When $q = 0$, obviously $\gamma_m = 2\pi mi$. Thus in this model there is no self-oscillatory instability.

When $q >> 2\pi m$, we can approximately find $\mathrm{Re}\gamma_m$:

$$\operatorname{Re}\gamma_m = -\int_0^1 \frac{q(\xi)}{k(\xi)}(1-\cos 2\pi m\xi)\,d\xi. \qquad (12)$$

In a resonator with rotating field, pumping leads to attenuation of perturbations. The onset of instability in an ordinary unstable resonator is due to inhomogeneous distribution of intensity over the cross section.

Exchange of excitations between N_2 and CO_2 also leads to damping of perturbations in a resonator with rotating field. In the model with exchange saturation (4) it is convenient to convert to the following dimensionless variables: $k_s = (x_C/x_N)2L\sigma n_N/(M-1)$, $u_s = \sigma/\tau_{NC}/\hbar\omega$, $\tau = tv/l$, $\xi = x_C l$, $\alpha_s = x_C l/(x_N v\tau_{NC})$, in which equation (4) takes the form

$$\partial k_s/\partial\tau - \partial k_s/\partial\xi = -\alpha_s u_s k_s/(1+u_s). \qquad (13)$$

The conditions at the resonator input and on its axis are written as follows:

$$k_s(1) = k_0; \quad k_s(0) = d(1+u_s). \qquad (14)$$

Using the linear theory of stability of the steady-state solution of (13), (14) we find the dispersion equation for γ (see (8)):

$$\exp(-\gamma) = 1+\gamma(1+u_{sc\tau})/\alpha_s, \qquad (15)$$

which can be approximately solved in two extreme cases:

$$\gamma_m = \begin{cases} 2\pi m i\left(\dfrac{\alpha_s-1}{\alpha_s}\right) - \dfrac{[2\pi m(\alpha_s-1)]^2}{2\alpha_s^4}(1+u_s)^2, & |\gamma_m| \ll \alpha_s; \qquad (16) \\ 2\pi i\left(m-\dfrac{1}{4}\right) - \ln\left[\dfrac{2\pi(m-1/4)}{\alpha_s}(1+u_s)\right], & |\gamma_m| \gg \alpha_s. \qquad (17) \end{cases}$$

4. Let us go on to answer the question of the influence that pumping has on self-oscillatory instability [Ref. 1]. To describe the field structure in an unstable resonator we take a quasi-one-dimensional geometric model that was proposed in Ref. 1, valid for $M-1 \ll 1$, $N_{eq} \gg 1$ (where N_{eq} is the equivalent Fresnel number). The equation for the overall intensity in this model takes the form

$$\frac{1}{x^{d-1}}\frac{\partial(x^d I)}{\partial x} = \frac{2L\sigma n_C}{M-1} I. \qquad (18)$$

(For spherical mirrors ($d = 2$) equation (18) is written for a straight line along the flow passing through the axis of the resonator). In dimensionless variables we get

$$\xi du/d\xi = (k-d)u. \qquad (19)$$

Attempts to get a steady-state solution in explicit form have so far been unsuccessful, and in the linear theory of stability (see (8)) now $\tilde{u}(\xi)$ satisfies the equation

$$\xi d\tilde{u}/d\xi = (k_{c\tau}-d)\tilde{u} + u_{c\tau}\tilde{k}. \qquad (20)$$

System of equations (9), (20), with conditions (10) can be reduced to a boundary value problem for an equation of second order for the quantity

$$\Phi(\xi) = \exp\left[-\frac{1}{2}\int_1^{\xi}\left(\gamma + \frac{1}{\eta} + u_{cr}\right)d\xi_1\right] \times$$
$$\times \int_1^{\xi} k_{cr}\tilde{u}(\xi_1)\exp\left[-\int_1^{\xi_1}\left(\gamma + \frac{1}{\eta} + u_{cr}\right)dy\right]d\xi_1.$$

The equation takes the form

$$\frac{d^2\Phi}{d\xi^2} + \Phi\left[-\frac{1}{4}\left(\gamma + \frac{1}{\eta} + u - \frac{d\ln(uk)}{d\xi}\right)^2 + \right.$$
$$\left. + \frac{1}{2}\frac{d}{d\xi}\left(\frac{d\ln(ku)}{d\xi} - u\right) - \frac{1}{\xi}\frac{dk}{d\xi}\right] = 0. \qquad (21)$$

Its solutions satisfy the boundary conditions $\Phi(0) = \Phi(1) = 0$. Multiplying (21) by Φ^*, integrating and taking the real part from the resultant equation we get

$$\mathrm{Re}\,\gamma = \frac{\left(-\int_0^1 \frac{q}{k}\Phi\Phi^* d\xi + \int_0^1 \Phi\Phi^* \frac{d\ln u}{d\xi}d\xi\right)}{\int_0^1 \Phi\Phi^* d\xi}. \qquad (22)$$

Expression (22) implicitly determines the increment of development of instability since the function Φ, generally speaking, is unknown. However, if the gain of the medium at the input is close to the threshold gain, $k_0 - d \ll 1$, and pumping is small, $\int_0^1 q(\xi)d\xi \ll 1$, then $|\mathrm{Im}\gamma| >> |\mathrm{Re}\gamma|$ and the eigenfunctions of the perturbations are found

$$\Phi_m(\xi) = \sin(\pi m\xi), \quad \mathrm{Im}\gamma_m = 2\pi m i. \qquad (23)$$

Since the coefficients of $|\Phi_m|^2$ in (22) are small, in order to find $\mathrm{Re}\gamma_m$ the zero approximation in calculation of Φ_m is sufficient. As a result we get

$$\mathrm{Re}\,\gamma_m = 2\int_0^1 \left(\frac{1}{u_{cr}}\frac{du_{cr}}{d\xi} - \frac{q(\xi)}{k_{cr}}\right)\sin^2(\pi m\xi)\,d\xi. \qquad (24)$$

Expression (24) defines the region of stability, the frequencies of developing perturbations and the rate of their increase. In particular, if pumping is uniform over the cross section of the resonator, $q = (d+\Delta)/\eta$ and $k_0 = d + \Delta$ when $\Delta \ll 1$, then $\mathrm{Re}\gamma_m$ is independent of the number of the mode of perturbation: $\mathrm{Re}\gamma_m = -1/\eta + \Delta$. In dimensionless variables $\mathrm{Re}\gamma_m = \frac{v}{l}\left(\frac{2Lk_{in}}{M-1} - d - \frac{l}{v\tau_p}\right)$. When pumping along the flow is inhomogeneous, preferential development of high-frequency perturbations is possible.

Let $k_{in} = d$, and let the pumping be concentrated on a small section halfway between the edge of the mirror and the axis of the resonator. Then perturbations will develop with a frequency that is a multiple of $2v/l$.

Such distribution of pumping leads to modulation of the intensity of the output emission with a period equal to half the time of flight τ_{pf}. From (22) we can get an expression for the rate of development of high-frequency perturbations at $k_{CT}(\xi)$, $q(\xi)$ (not necessarily small). At high frequencies ($m \to \infty$), the eigenfunctions of the perturbations coincide with (23) and

$$\operatorname{Re}_{m\to\infty}\gamma_m = -\int_0^1 \frac{q(\xi)}{k(\xi)}\,d\xi + \ln\frac{u_{cT}(1)}{u_{cT}(0)}. \qquad (25)$$

The inequality $\ln\frac{u(1)}{u(0)} > \int_0^1 \frac{q(\xi)}{k(\xi)}\,d\xi$ is a sufficient condition of instability of steady-state laser operation. From the simple model of an active medium in an unstable resonator considered above we can draw the following conclusions.

An increase in parameter $q = \frac{2Ll}{v}\frac{\sigma Q_N}{M-1}\frac{x_C}{x_N}$ leads to stabilization of the steady state of laser operation. This conclusion explains the experimental data of Ref. 2 In which a reduction of M led to attenuation of pulsations.

The frequencies of developing perturbations depend on the distribution of pumping and on k_{in}. A reduction of k_{in} stabilizes the working mode of the laser.

For stability of steady-state laser operation with respect to small perturbations, it is necessary at least that the inequality

$$\ln\frac{I(l)}{I(0)} < \frac{x_C}{x_N}\frac{1}{v}\int_0^l \frac{Q_N(x)}{n_C(x)}\,dx$$

be satisfied.

5. Let us consider the question of the way that saturation of exchange N_2-CO_2 affects the development of self-oscillatory instability. To simplify the equations we introduce the new function

$$\varphi(\xi) = \int_1^{\xi} \frac{k_s\dot{u}_s}{1+u_s}\exp\left[-\int_1^{y}\left(\gamma + \frac{\alpha_s u_s}{1+u_s}\right)dy_1\right]dy.$$

For this function, from linearized equations (13), (18) with conditions (14) we can get the second-order equation

$$\xi\left[\frac{d^2\varphi}{d\xi^2} + \frac{d\varphi}{d\xi}\left(\gamma + \frac{\alpha_s u_s}{1+u_s} - \frac{d}{d\xi}\ln\frac{k_s u_s}{1+u_s}\right)\right] = -\frac{k_s u_s}{(1+u_s)^2}\frac{d\varphi}{d\xi} + \frac{\alpha_s k_s u_s}{(1+u_s)^3}\varphi \qquad (26)$$

with conditions

$$\varphi(1) = 0,\ \left.\frac{d\varphi}{d\xi}\right|_{\xi=0} = \frac{\alpha_s}{1+u_s}\varphi. \qquad (27)$$

The problem of stability is solved by finding the eigenvalues γ_n and the eigenfunctions $\phi_n(\xi)$ of boundary value problem (26), (27). This problem can be solved analytically in the case where the lasing threshold is slightly exceeded ($k_0 - d << 1$) and at high frequencies ($|\gamma_n| >> 1$). In these cases we can use perturbation theory as in Ref. 9.

Let $k_0 - d = \Delta << 1$. With accuracy to terms of the order of Δ from (26) we get

$$\frac{d^2\varphi}{d\xi^2} + \gamma \frac{d\varphi}{d\xi} = \frac{\Delta\alpha_s}{1+\alpha_s}\frac{d\varphi}{d\xi} - \frac{1}{\xi}\left(\frac{\Delta}{1+\alpha_s}\frac{d\varphi}{d\xi} - \frac{\Delta\alpha_s}{1+\alpha_s}\varphi\right). \tag{28}$$

When $\Delta = 0$, the eigenfunctions ϕ_{0n} that satisfy boundary conditions (27) take the form $\varphi_{0n} = e^{-\gamma_{0n}\xi} - e^{-\gamma_{0n}}$, while the eigenvalues γ_{0n} are solutions of transcendental equation (15). Applying perturbation theory with respect to the small parameter Δ and following Ref. 9, we get

$$\operatorname{Re}\gamma_n = -\frac{|\gamma_{0n}|^2}{2\alpha_s^2}(1 + u_s(0))^2 + \frac{\Delta\alpha_s}{1+\alpha_s},\ \alpha_s \gg |\gamma_{0n}|. \tag{29}$$

The eigenfunctions and eigenvalues take the form

$$\varphi_n = e^{-\gamma_n\xi} - e^{-\gamma};$$

$$\gamma_n = 2\pi n i\left(\frac{\alpha_s - 1}{\alpha_s}\right) - \frac{2\Delta\alpha_s}{1+\alpha_s}\frac{i}{2\pi n}\int_0^{2\pi n}\frac{1-\cos x}{x}dx + \frac{\Delta\alpha_s}{1+\alpha_s} - \frac{[2\pi n(\alpha_s - 1)]^2}{2\alpha_s^4}. \tag{30}$$

The equation $\operatorname{Re}\gamma_1 = 0$ defines the boundary of the region of stability of the steady-state solution. When $\alpha_s >> 2\pi$, the equation of the boundary takes the form $\alpha_{sk} = 2\pi\sqrt{2\Delta}$. For a CO_2-N_2 mixture we get the condition of stability of the steady-state mode of operation of a fast-flow laser $x_C\tau_{tf}/(x_N\tau_{NC}) < 2\pi/\sqrt{2\Delta}$. Numerical calculations in Ref. 6 showed an abrupt increase in the parameter α_{sk} with approach to the lasing threshold.

If the saturation parameter is sufficiently large, $2\pi n/\sqrt{2\Delta} < \alpha_s < 2\pi(n+1)/\sqrt{2\Delta}$, then perturbations will develop with all frequencies right up to the n-th harmonic. Therefore it can be expected that the duration of emission pulses $\tau_и$ in the self-oscillatory mode will be no less than $2\pi l/v\alpha_s\sqrt{2\Delta}$. For a CO_2-N_2 gas mixture the duration of the emission pulses does not depend on the time of flight, but rather is determined only by the

the parameters of the mixture and the excess over the lasing threshold $\tau_и \approx \frac{2\pi}{\sqrt{2\Delta}}\frac{x_N}{x_C}\tau_{CN}$.

In examining the problem of the stability of the steady-state mode of fast-flow laser operation with respect to small perturbations of high frequency, we can use perturbation theory in (26) with respect to the parameter $1/|\gamma|$ without assuming smallness of $k_0 - d$.

treatment analogous to the preceding gives

$$\begin{aligned} \mathrm{Re}\gamma_n &= \ln(k_0/d) \quad \text{when } |\gamma_n| \ll \alpha_s; \\ \mathrm{Re}\gamma_n &= -\ln(|\gamma_n|/\alpha_s) \text{ when } |\gamma_n| \gg \alpha_s. \end{aligned} \tag{31}$$

Here $|\gamma_n| = |\mathrm{Im}\gamma_n| = 2\pi n$; $|\gamma_n| \gg k_0$; $\ln(k_0/d) \gtrsim 1$. The duration of emission pulses in the automodulation mode can be determined from expression (31) for the increment of instability. Since perturbations will develop with frequencies right up to $\omega_n \approx \alpha_s k_0/d$, then $\tau_и \approx 2\pi d\tau_{tf}/(\alpha_s k_0)$.

For a CO_2-N_2 mixture $\tau_и \approx 2\pi d x_N \tau_{NC}/(k_0 x_C)$. An increase in k_0 leads to a reduction in the duration of emission pulses. In the case of an arbitrary excess over the threshold, the criterion of stability of the steady-state mode obviously has the form $\alpha_{sk} \approx 2\pi$, which agrees well with the numerical criterion from Ref. 6 written in the beginning of the paper.

6. Thus we have established on the basis of simplified kinetic models of a medium that account for pumping, exchange saturation or relaxation of the lower level that self-oscillatory instability [Ref. 1] does not occur in an unstable resonator with rotating field [Ref. 8], and in an ordinary unstable resonator it can be suppressed by selecting the parameters of the working medium in the resonator. Explicit conditions have been found for these parameters for which instability does not develop. For supercritical modes an estimate has been found for the number of developing modes of perturbations and the duration of self-oscillation spikes.

REFERENCES

1. Yu. A. Dreyzin, A. M. Dykhne, PIS'MA V ZHURNAL EKSPERIMENTAL'NOY I TEORETICHESKOY FIZIKI, Vol 19, 1974, p 718.

2. M. J. Yoder, D. R. Ahouse, APPL. PHYS. LETTS., Vol 27, 1975, p 673.

3. A. V. Artamonov, V. G. Naumov, KVANTOVAYA ELEKTRONIKA, Vol 4, 1977, p 178.

4. H. Mirels, APPL. PHYS. LETTS., Vol 28, 1976, p 612.

5. M. L. Alme, APPL. PHYS. LETTS., Vol 29, 1976, p 35.

6. Yu. A. Dreyzin, A. M. Dykhne, A. P. Napartovich, Yu. M. Panchenko, in: "Tezisy Vtorogo Vsesoyuznogo simpoziuma po gazovym lazeram" [Abstracts of the Second All-Union Symposium on Gas Lasers], Novosibirsk, 1975.

7. A. A. Vedenov, A. P. Napartovich, TEPLOFIZIKA VYSOKIKH TEMPERATUR, Vol 12, 1974, p 952.

8. Yu. A. Anan'yev, PIS'MA V ZHURNAL TEKHNICHESKOY FIZIKI, Vol 4, 1978, p 372.

9. V. V. Likhanskiy, A. P. Napartovich, KVANTOVAYA ELEKTRONIKA, Vol 4, 1977, p 1353.

6610
CSO: 1862

UDC 621.378.325

EXPERIMENTAL STUDY OF THE WAY THAT RHODAMINE-6G LASER EMISSION ACTS ON ALUMINUM

Moscow KVANTOVAYA ELEKTRONIKA in Russian Vol 7, No 2(92), Feb 80
pp 349-354 manuscript received 1 Jul 79

[Article by A. A. Bakeyev, B. A. Barikhin, V. V. Borovkov, L. A. Vasil'yev, L. I. Nikolashina, A. I. Pavlovskiy, N. V. Prokopenko, L. V. Sukhanov, A. I. Fedosimov and V. I. Yakovlev]

[Text] It is known [Ref. 1, 2] that the coefficient of reflection of metals decreases with transition from infrared to visible wavelengths. In this connection there is a good outlook for using powerful lasers in the visible band for machining materials. The experimental data that we have on the way that powerful emission in the visible band acts on materials has been obtained mainly by using ruby lasers that operate either in the free emission mode ($\tau_p \approx 1$ ns) or in the Q-switched mode ($\tau_p \approx 10$ ns). The range of exposure durations of 1-10 μs for the visible band has been inadequately studied. This time interval can be provided in particular by dye lasers.

Ref. 3 describes the first experiments to study the action of Rhodamine-6G laser emission with a wavelength of $\lambda = 0.58$ μm on various materials. The maximum radiation flux density in these experiments did not exceed $q = 3$ MW/cm^2.

In our research an investigation was made of the way that emission from a laser based on a solution of Rhodamine-6G in ethanol with lasing pulse duration $\tau_p \approx 8$-10 μs on the 0.1 level acts on aluminum in the range of average radiation power densities of $5 \leqslant q \leqslant 60$ MW/cm^2. Principal attention was focused on studying the plasma flare, which may have a considerable effect on the results of the action at high values of q.

Description of the Experimental Facility

A diagram of the experimental facility is shown in Fig. 1. Laser 1 based on an ethanol solution of Rhodamine-6G dye was used as the source of

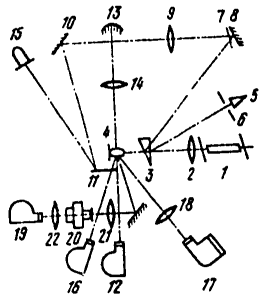

Fig. 1. Diagram of the experimental facility

powerful radiation in the visible band. The design of the laser is described in detail in Ref. 4, 5. The laser emission was focused by lens 2 with focal length of f = 500 mm on the surface of aluminum specimen 4 located in its focal plane. Part of the emission energy was directed by the front face of wedge 3 to an energy meter type IKT-1M 5 with input port also located in the focal plane of lens 2 with restriction by interchangeable irises 4. The emission reflected by the rear face of wedge 3, after passing through an optical system made up of the air wedge formed by mirrors 7 and 8, lens 9 and rotating mirror 10, produced a series of images of the focusing spot on matte plate 11 in a scale of 1.5:1 with a known attenuation factor of one image relative to another. Plate 11 was located in a plane passing through the axis of the laser beam in such a way that on the one hand there was no interference with development of the flare arising on the specimen, and on the other hand the plate and flare were in the field of view of SFR-M streak camera 12.

To get information on the space-time distribution of temperature and absorbing properties of the plasma, streak camera 12 photographed the flare in the spectral range of 0.488 ± 0.002 μm isolated by an interference filter with the use of a self-brightening arrangement [Ref. 6] consisting of concave reflector grating 13 and lens 14. A metal mirror with milled nonreflecting (chemically oxidized) strips was used as the grating. A dielectric coating was sputtered on the reflecting strips with reflectivity of 95% on a wavelength of $\lambda = 0.488$ μm. The temperature measurements were made by a homochromic photometry technique. Thus the spatial distribution of equilibrium temperature T_{eq} and brightness temperature T_{br} in the flare, as well as the distribution of laser emission energy in the focusing spot were determined with a time resolution of 0.5 μs by using streak camera 12.

FEK-14 coaxial photocell 15 was used to register the time behavior of the laser pulse. SFR-M streak camera 16 operated in the photoscan mode at a speed of 3 km/s and was used for determining the rate of propagation of the luminescent front of the flare opposite to the laser beam. Time-integrated but spatially resolved spectra of the flare radiation were produced by ISP-51 spectrograph 17 with lens 18 at the output slit forming an image of the axial zone of the flare.

In a number of experiments the spectrum of the flare was taken at 440-470 nm with time resolution of 2 μs. To do this, lens 21 formed an image of the axial region of the flare at the output slit of monochromator 20 (MDR-2). In the described experiments, the output slit of the monochromator was removed. The magnified virtual image of the flare spectrum formed by lens 22 was photographed by SFR-M streak camera 19.

The mass removed by exposure was determined by weighing the specimens on an analytical balance before and after irradiation.

Results of the Experiments

Fig. 2a shows an oscillogram of the lasing pulse. Fig. 2b shows the results of measurements of integrated and two "instantaneous" distributions of energy on the surface of the specimens. The integral distribution was found by simultaneous measurement of the total laser radiation and the part isolated by irises 6 of different diameters (see Fig. 1) placed in the focal plane of lens 2. The instantaneous distribution was determined by microphotometric measurement of negatives of the focusing spot obtained on streak camera 12. It was found that an appreciable increase in the divergence of laser emission (the diameter of the focusing spot) took place up to t = 2 μs. After that there was practically no change in the divergence.

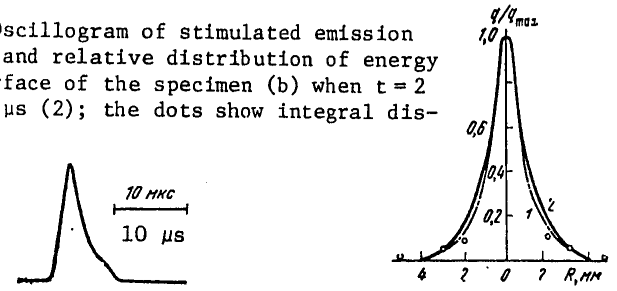

a b

Fig. 2. Oscillogram of stimulated emission pulse (a) and relative distribution of energy on the surface of the specimen (b) when t = 2 (1) and 7 μs (2); the dots show integral distribution

It is clear from Fig. 2b that the energy density in the central region of a focusing spot 4 mm in diameter is nearly an order of magnitude greater than the corresponding quantity in the wings of the distribution. It can be assumed on this basis that the nature of the effect in the described experiments was determined by the emission flux density in the central zone. Therefore hereafter, where not specifically stipulated in the presentation and discussion of experimental results we will relate all measured quantities to the average values of the emission flux density in the central exposure zone 4 mm in diameter.

Visual examination of irradiated specimens showed that removal of the mass of material takes place chiefly from the central zone of about 4 mm. The absence of noticeable droplets of melt on specimens and on the parts of the installation shows that most of the material is carried off in the vapor state. In the range of emission flux densities of 5-60 MW/cm^2 the specific removal of mass for aluminum specimens was $(2\text{-}4)\cdot10^{-2}$ mg/J.

Negatives obtained by streak cameras 12 and 16 (see Fig. 1) were used to determine the time of delay Δt in appearance of the flare relative to

the onset of stimulated emission, and also the area S of the focusing spot at the instant of onset of the flare. The emission energy ΔE incident on the surface of the specimen before onset of the flash, and also the average energy density $E_0 = \Delta E/S$ were found from oscillograms of the lasing pulse and the delay time. The measurement result are summarized in Table 1.

TABLE 1

№ п/п	Δt, мкс μs	S, см²	ΔE, Дж J	E_0, Дж/см² J/cm²	$k \cdot 10^{-18}$, Вт/(см·с)² W/(cm·s)²
1	1,5	0,04	0,7	10,5	0,9
2	1,0	0,12	1,4	11,5	2,3
3	1,7	0,13	1,9	14,5	1,0
4	1,2	0,10	1,1	10,4	2,0
5	0,7	0,03	0,3	10,2	3,0

Here $k = 2\Delta E/(S\Delta t^2)$ is the rate of change of emission intensity. It can be seen from Table 1 that in the investigated range of rates of change of emission intensity the flash of aluminum vapors takes place at about the same energy density on the target $E_0 \approx (10\text{-}12)$ J/cm².

Immediately after the flash arises the brightness of the flare along the axis is uniform. Then the flare begins to separate into three distinct regions differentiated from one another by brightness of luminescence (Fig. 3). The first region, located directly on the target, has a height

Fig. 3. Photograph of plasma flare with delay of ~0.5 μs (a) and photoscan of motion of the leading edge of the flare (b) [1 мкс = 1 μs]. At the lower right in photograph *a* is the laser flash

of no more than 1.5-2.0 mm, and a transverse dimension approximately equal to the diameter of the crater left by the radiation on the target. The height of the second region with luminescence intensity considerably lower than on the target, at first increases at a rate of about 0.5 km/s, and then practically ceases changing in the middle of the lasing pulse. In the third region the brightness of the flare once again increases, and its boundary, which coincides with the leading luminescent front of the flare, moves counter to the laser beam at a velocity of up to 3 km/s. Such a flare structure is typical of an evaporative mode of action with appreciably two-dimensional dispersal of the resultant vapor [Ref. 7, 8].

The maximum velocities v_{max} of propagation of the leading edge of the flare were reached practically simultaneously with the lasing maximum, and at this point the height of the flare above the target did not exceed the dimensions of the focusing spot (see Fig. 3b). It can therefore be assumed in a first approximation that dispersal of the flare is flat up to this instant.

Fig. 4 shows the measured values of v_{max} as a function of the maximum emission flux q_{max} in the spot. The principal error in determination of the dependence $v_{max}(q_{max})$ involves determination of the values of q_{max}, where the error may reach ±50%. The solid line on the figure denotes the rate v of propagation of a subsonic radiation wave as a function of q, which according to Ref. 9 is described by the expression

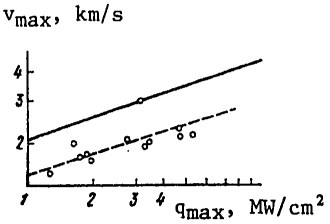

Fig. 4. Dependence of v_{max} on q_{max}

$$v \approx 0{,}95\, q^{1/4},$$

where v is in km/s and q is in MW/cm^2. With consideration of measurement errors, the experimental values of v_{max} lie below the values calculated from the cited formula.

Analysis of the time-integrated spectra has shown that the emission spectrum of the plasma flare contains, in addition to lines of ionized aluminum Al-II and Al-III, also molecular bands of AlO that show up on the stage of decay of the plasma flare. This is confirmed by the emission spectra of a flare in the interval of 0.446-0.466 μm taken with spatial and time resolution of 1 mm and 2 μs respectively. As can be seen from

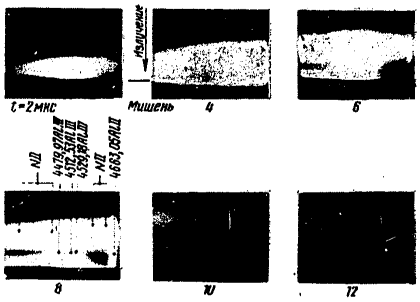

Fig. 5. Photographs of emission spectra of the axial zone of a flare with time resolution of 2 μs

Key to Russian words:

мкс - microseconds
Мишень - Target
Излучение - Emission

Fig. 5, in the first 2-4 μs the spectrum is fairly uniform over the height of the flare, and consists of continuous emission and strongly broadened lines of Al-II and Al-III that are practically indistinguishable from the continuous background. By 4-8 μs (depending on the injected power) a quasi-steady jump has been formed, and three regions can be distinguished in the flare with differing spectral composition and intensity. In this time period the emission spectrum at the surface of the target is mainly continuous with strongly broadened lines of Al-II and Al-III. However, the intensity of the continuous spectrum is somewhat lower than in the initial instants of exposure. In the region of two-dimensional supersonic dispersal (between the surface of the target and the compression jump) there is a drop in the intensity of continuous emission, and lines of ionized aluminum can be clearly seen against this background. In the compression jump and throughout the region right up to the leading edge of the flare an intense continuous spectrum is observed with strongly broadened lines of ionized aluminum. In the narrow zone close to the leading edge of the flare, lines of ionized nitrogen are observed that have not been detected on integrated spectra. Decay of plasma formation takes place after termination of the lasing pulse. In the spectra corresponding to this time period (10-12 μs) the intensity of continuous emission drops off at a rate that increases on the surface of the target.

Thus the spectral measurements completely confirmed the evaporative nature of exposure in our experiments at emission flux densities up to 60 MW/cm^2. The results of measurement of the temperature profile in one of the experiments are summarized in Table 2 (E/S = 122 J/cm^2).

TABLE 2

t, мкс μs	Номер зоны (Zone number) I T_{br}	I T_{eq}	I	I	I	II T_{br}	III T_{br}	III T_{eq}	III	III	III
	$T_я \cdot 10^{-3}$, K	$T_p \cdot 10^{-3}$, K	$\tau_\perp$	k, см$^{-1}$	$\tau_\parallel$	$T_я \cdot 10^{-3}$, K	$T_я \cdot 10^{-3}$, K	$T_p \cdot 10^{-3}$, K	$\tau_\perp$	k, см$^{-1}$	$\tau_\parallel$
1,0	25,6	29,2	1,6	8,1	0,8						
1.5	30,0	38,5	1,1	4,7	0,7	31,0					
2,0	26,0	38,5	0,7	2,2	0,4	22,5					
2,5	22,0	27,5	1,1	2,0	0,2	17,2	29,6	37,5	1,1	2,8	0,5
3,0	21,0	25,4	1,2	2,4	0,2	15,6	30,5	37,0	1,4	2,8	0,6
3,5	26,0	35,0	0,9	1,6	0,2	15,6	32,6	39,5	1,4	2,8	0,6
4,0	—	—	—	—	—	15,4	28,8	34,5	1,4	2,3	0,6
4,5	29,0	28,5	0,7	1,3	0,2	14,8	27,5	33,5	1,2	2,0	0,6
5,5	—	—	—	—	—	—	21,5	26,0	1.2	1,6	0,5

Note: t is time from lasing onset; $\tau_\perp$ and $\tau_\parallel$ are the optical thicknesses of the plasma flare in the directions perpendicular and parallel to the laser beam; k is the coefficient of absorption in the plasma flare on $\lambda = 0.488$ [μm]. The cross sections in which the temperature measurements were made are shown in Fig. 5.

It can be seen from Table 2 that in the initial instants of exposure (before formation of the quasi-steady compression jump), high temperatures form in the plasma flare (up to about $4 \cdot 10^4$ K). After formation of the jump, the temperature maximum shifts closer to the front, and the plasma temperature on the target drops sharply. In the zone of two-dimensional dispersal (zone II), the brightness temperatures are much lower than on the target and beyond the compression jump.

Data on the optical thicknesses of the plasma flare are noteworthy. Up until formation of the quasi-steady compression jump the optical thickness for laser emission parallel to the beam axis is 0.7-0.9. After formation of the jump, the optical thickness of the plasma close to the target (zone I) decreases abruptly to values of 0.1-0.2, while beyond the compression jump (zone III) the value of $\tau_{\parallel}$ remains practically constant and equal to 0.5-0.6.

With such optical thicknesses in the plasma flare, an appreciable part (up to 30%) of the incident emission is absorbed, and a further increase of energy or duration of the laser pulse may cause a transition to conditions involving appreciable shielding of the target. This is also shown by ionized air lines that appear close to the flare front.

Thus a power density $q = 60$ MW/cm^2 is apparently the limit for machining metal by emission with $\lambda = 0.58$ μm with focusing spot diameters of more than 0.5 cm. With a reduction of the focusing spot, the upper limit of existence of the evaporative mode will shift toward higher values of q.

REFERENCES

1. Dzh. Key, T. L. Lebi, "Tablitsy khimicheskikh i fizicheskikh postoyannykh" [Tables of Chemical and Physical Constants], Moscow, Fizmatgiz, 1962, p 94.

2. V. P. Tychinskiy (ed.), "Primeneniye lazerov" [Use of Lasers], Moscow, Mir, 1974.

3. V. K. Goncharov, L. Ya. Min'ko, S. A. Mikhnov, V. S. Strizhnev, KVANTOVAYA ELEKTRONIKA, No 5, 1971, p 112.

4. F. N. Baltakov, B. A. Barikhin, L. V. Sukhanov, PIS'MA V ZHURNAL EKSPERIMENTAL'NOY I TEORETICHESKOY FIZIKI, Vol 19, 1974, p 300.

5. A. A. Bakeyev, B. A. Barikhin, V. V. Voronkov, ZHURNAL PRIKLADNOY SPEKTROSKOPII, Vol 31, 1979, p 242.

6. V. K. Goncharov, L. Ya. Min'ko, Ye. S. Tyunina, A. N. Chumakov, KVANTOVAYA ELEKTRONIKA, No 1(13), 1973, p 56.

7. V. K. Goncharov, L. Ya. Min'ko, Ye. S. Tyunina, ZHURNAL PRIKLADNOY SPEKTROSKOPII, Vol 13, 1970 p 707.

8. V. A. Batanov, F. V. Bunkin, A. M. Prokhorov, V. B. Fedorov, ZHURNAL EKSPERIMENTAL'NOY I TEORETICHESKOY FIZIKI, Vol 63, 1972, p 1240.

9. V. I. Bergel'son, T. V. Loseva, I. V. Nemchinov, ZHURNAL PRIKLADNOY MEKHANIKI I TEKHNICHESKOY FIZIKI, No 4, 1974, p 22.

6610
CSO: 1862

UDC 621.378.3;373.8

PARTICULARS OF STIMULATING EMISSION IN VAPORS OF COMPLEX ORGANIC COMPOUNDS

Moscow KVANTOVAYA ELEKTRONIKA in Russian Vol 7, No 2(92), Feb 80
pp 383-390 manuscript received 18 Jul 79

[Article by G. A. Abakumov, S. A. Vorob'yev, Yu. Lademan and A. P. Simonov, Scientific Research Physicochemical Institute imeni L. Ya. Karpov, Moscow]

[Text] In contrast to the case of solutions, stimulated emission in vapor has been achieved only for a limited number of organic compounds [Ref. 1-4] and only with pumping by monopulses on the second harmonic of ruby laser emission (pumping wavelength $\lambda_p = 347$ nm), the third harmonic of a neodynium laser ($\lambda_p = 353$ nm) and nitrogen laser emission ($\lambda_p = 337$ nm). The emission characteristics of organic compounds that lase in the gas phase (threshold and efficiency of stimulated emission) are poorer than the corresponding characteristics of the same compounds in solution. The poor emission characteristics or absence of lasing in vapor is usually attributed to the low photostability of organic compounds in vapors, and to products of photodissociation that absorb on the lasing wavelength λ_{se} [Ref. 2-8]. When emission characteristics in vapor are interpreted in theoretical analysis, consideration is also taken of losses on λ_{se} that are usual for organic compounds, e. g. the losses due to triplet-triplet absorption [Ref. 9-11].

At the present time the theoretical analysis of the process of stimulated emission in organic vapors is being done on the basis of equations that have ordinarily been used to analyze stimulated emission in solutions [Ref. 8, 11, 12]. Such an approach has a considerable disadvantage: no consideration is taken of the fundamental difference between the properties of molecules in solution and in the gas phase. In contrast to solutions, in vapors one of the principal characteristics of complex molecules [Ref. 13] is storage of vibrational energy U in the ground state and in excited electron states. The magnitude of U appreciably determines all spectroscopic and photochemical characteristics of the molecules: absorption and fluorescence spectra, lifetime of the excited

state, quantum yields of fluorescence, triplet states and photodissociation. Even when there is no induced absorption on λ_{se} or λ_p, the U of the molecules in the ground and excited states may be appreciably changed during lasing by successive acts of excitation and emission, which leads to a strong change in the lasing characteristics of the system.

To analyze lasing in organic vapors in this paper, we take the simplest model of a system of two electron levels broadened by vibrational sublevels of the ground level (1) and the excited singlet level (2). The populations of active molecules in each of electron levels 1 and 2 are characterized by time-dependent distributions $n_1(U,t)$ and $n_2(U,t)$ with respect to vibrational energy. It is also assumed that the active molecules are surrounded by molecules of neutral gas with which vibrational energy is exchanged at a rate that depends on the number p of collisions between molecules in a unit of time. Induced absorption of all types is disregarded. For the sake of simplicity, pumping through the active zone is taken as uniform. The model reflects the specifics of the gas phase in the case that is most favorable for lasing.

For the assumed model, the kinetics of populations $n_1(U,t)$ and $n_2(U,t)$ and the spectral density of the total number of photons of stimulated emission $\gamma(\nu,t)$ in the resonator can be described by the system of equations

$$\frac{\partial n_2(U,\ t)}{\partial t} = -\left[p_2(U) + p + \frac{c}{L}\int_{-\infty}^{\infty}\gamma(E,\ t)\,\sigma_{21}(U,\ E)\,dE + f(t)\,\sigma_{21}(U,\ E_{\text{н}})\right]\times$$
$$\times\, n_2(U,\ t) + f(t)\,\sigma_{12}(U - E_{\text{н}},\ E_{\text{н}})\,n_1(U - E_{\text{н}},\ t) +$$
$$+\frac{c}{L}\int_{-\infty}^{\infty}\gamma(E,\ t)\,\sigma_{12}(U-E,\ E)\,n_1(U-E,\ t)\,dE + pn_2(U+\Delta U,\ t);$$
$$\frac{\partial n_1(U,\ t)}{\partial t} = -\left[f(t)\,\sigma_{12}(U,\ E_{\text{н}}) + p + \frac{c}{L}\int_{-\infty}^{\infty}\gamma(E,\ t)\,\sigma_{12}(U,\ \varphi)\,dE\right]n_1(U,\ t) +$$
$$+\frac{c}{L}\int_{-\infty}^{\infty}\gamma(E,\ t)\,\sigma_{21}(U+E,\ E)\,n_2(U+E_{\text{г}},\ t)\,dE + f(t)\,\sigma_{21}(U+E_{\text{н}},\ E_{\text{н}})\,n_2(U+$$
$$+E_{\text{н}},\ t) + \int_{-\infty}^{\infty}p_{21}(U+E,\ E)\,n_2(U+E,\ t)\,dE + pn_1(U+\Delta U,\ t);$$
$$\frac{\partial\gamma(E,\ t)}{\partial t} = \gamma(E,\ t)\,\frac{c}{L}\left[K_{\text{у}}(E,\ t) - K_{\text{н}}(E,\ t) - \frac{1}{2}Q\right], \qquad (1)$$

where $K_{\text{у}} = l\int\sigma_{21}(U,\ E)\,n_2(U,\ t)dU$, $K_{\text{н}} = l\int\sigma_{12}(U,\ E)\,n_1(U,\ t)\,dU$ are the gain and loss respectively in system of levels 2 and 1; L and l are the respective lengths of the resonator and the active zone; c is the speed of light on λ_{se} in the resonator; Q is the value of constant losses in the resonator in one round trip.

The time dependence of the pumping photon flux density is taken as gaussian:

$$f(t)=f_0 \exp[-(t/t_0)^2]. \quad (2)$$

It is assumed that both active POPOP molecules and neutral gas molecules (nonane, dodecane) are complex and have a large number of vibrational degrees of freedom ($N \geqslant 50$). For such molecules the width δU of distribution of the molecules (both active and those of the extraneous gas) in the equilibrium state is small [Ref. 14], and therefore in doing the calculations it can be assumed that δU is much less than the characteristic changes of vibrational energy of the active molecules. In this case the change in vibrational energy ΔU of an active molecule during collision with molecules of neutral gas can be expressed in simplest form as

$$\Delta U(U)=\alpha(U-U_0), \quad (3)$$

where U_0 is the equilibrium value of vibrational energy of the active molecules as determined by the temperature of the system; α is the accommodation coefficient equal to 0.05-0.20 for real systems [Ref. 13, 15].

The intensity of absorption or radiation of light quanta is described by the cross sections of absorption σ_{12} and stimulated emission σ_{21} that depend on the storage of vibrational energy in the corresponding electron state and the frequency ν of the absorbed or emitted light. The dependence of σ_{12} and σ_{21} on ν is conveniently represented as the dependence on the change of vibrational energy in the electronic transition $E = h\nu - E_0$, where E_0 is the energy of a purely electronic transition, so that E_p and E_{se} are the respective energies for frequencies of pumping ν_p and lasing ν_{se}.

The transition cross sections, in accordance with Ref. 14, can be written in the form

$$\sigma_{21(12)}(U, E)=\frac{a}{\sqrt{2E_sU/N}} \exp\left[-\frac{(E\mp E_s/2)^2}{2E_sU/N}\right], \quad (4)$$

where the plus and minus signs refer to quantities that describe emission and absorption of radiation; E_s is the Stokes shift between absorption and emission spectra; N is the number of degrees of vibrational freedom of the active molecule; a is a constant determined by the properties of the molecule. Relation (4) describes the experimentally observed change of the spectra of absorption and emission with increasing U (or temperature T): an increase in the width of the spectra with a corresponding reduction in their intensity at the maximum ($E = \mp E_s/2$) and an increase in overlap of the spectra. For the sake of simplicity of the calculations, it is assumed that the probability of radioactive deactivation of level 2 on the corresponding frequency $p_{21}(U,E)$ is related to $\sigma_{21}(U,E)$ by the expression

$$p_{21}(U, E)=\frac{8\pi}{h^3c^2}\left(E_0-\frac{E_s}{2}\right)^2\sigma_{21}(U, E). \quad (5)$$

in which the term $(E_0+E)^2$, which varies weakly within the limits of the fluorescence band, is replaced by the constant $(E_0 - E_s/2)^2$ which coincides with the former at the band maximum $E = -E_s/2$. The dependence of the total

rate of deactivation of fluorescence level 2 on the reserve vibrational energy U is written as [Ref. 13]

$$p_2(U)=p_{21}(1+\varkappa e^{\beta U}), \qquad (6)$$

where $p_{21}=\int p_{21}(U, E)\,dE=[8\pi^2/(h^3c^2)]\;a(E_0-E_s/2)^2$ is the total radiative rate of deactivation of level 2 that is independent of U; κ and β are empirical constants that characterize the increase in nonradiative decay of level 2 as U increases. It is assumed that as a result of nonradiative transition the molecules leave the two-level system completely, i. e. the total concentration of active molecules decreases. The products of nonradiative decay of level 2 (triplet molecules, products of dissociation) do not introduce additional losses on λ_{se}.

As can be seen from system of equations (1), the first two equations take account of losses on λ_{se} due to reabsorption of stimulated emission on transition $1 \to 2$, and depletion of fluorescence level 2 as a result of the forced transitions $2 \to 1$ on λ_p.

Under conditions of intensive excitation during a pumping pulse, the molecule undergoes several acts of excitation and emission of radiation. In doing so, its radiative energy in each act changes by the amounts E_p and $-E_{rad}$, which as a rule are both positive, which leads to an increase in the average reserve of vibrational energy, i. e. to effective heating of the molecules in both the ground and the excited state. This situation is considerably detrimental to the lasing characteristics of the system due to a drop in quantum fluorescence yield with increasing U, as well as to a reduction in the concentration of active molecules, an increase in the overlap of absorption and fluorescence spectra, and consequently of the losses on λ_{se}.

System (1) has been numerically analyzed by computer, using parameters close to experimental data for lasing of POPOP in vapor in the presence of neutral gases with pumping by monopulses of ultraviolet laser emission. Given below are the most typical results of calculation in which the following values of parameters were used: $p_2t_0 = 2.7$ (at a half-width of the pumping pulse $t_0 = 5$ ns the total radiative lifetime of the active molecule $1/p_{21} = 1.85$ ns); the equilibrium value of the vibrational energy $U_0 = 5E_s$; the parameters of nonradiative deactivation $\kappa = 0.54$; $\beta E_s = 1$ (at $E_s = 0.5$ eV, $N = 50$ the equilibrium values of the vibrational energy and temperature $U_0 = 2.5$ eV, $T_0 = 580$ K); the value of the cross section of absorption and amplification at the maxima for the equilibrium vibrational energy $\sigma_0=a/\sqrt{2E_sU_0N^{-1}} \approx 2\cdot10^{-16}$ cm^2; accommodation coefficient $\alpha = 0.05$; number of collisions with neutral gases pt_0 was varied over a a range of 0-1000 (which at $t_0 = 5$ ns corresponds to a change in pressure of the neutral gas from 0 to 25 atm at a collisional radius of 1 nm); coefficient of maximum gain $K=\sigma_0 n_0 l$ is taken as equal to 10, i. e. at l = 1 cm the total concentration of active molecules before pumping action ($t=-\infty$) $n_0 = 5\cdot10^{16}$ cm^{-3}, which corresponds to a pressure of about 4 mm Hg at $T_0 = 580$ K.

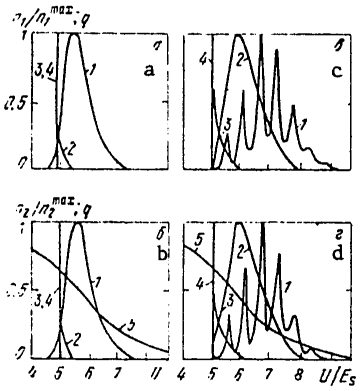

Fig. 1. U distributions of populations of the ground (a, c) and excited (b, d) states with (c, d) and without (a, b) stimulated emission at a neutral gas pressure P = 0 (1), 5 (2) and 25 (3) atmospheres and collision rates of $pt_0 = 0$ (1), 200 (2) and 1000 (3); Q = 1. Vertical line 4 shows the equilibrium distribution of curve 5 -- q(U)

Fig. 1 shows the distributions with respect to U for populations of the ground and excited states at different pressures of the neutral gas with and without stimulated emission in the system. It was assumed that the optical cavity was nonselective. The intensity of excitation $f_0\sigma_0 t_0 = 80$, i. e. for the given values of σ_0 and t_0 the flux density $f_0 = 8 \cdot 10^{25}$ cm$^{-2}\cdot$s^{-1} (or about 40 MW/cm^2 for $\lambda_p = 355$ nm). Pumping was on the frequency of the purely electronic transition, $E_p = 0$. The vertical lines at $U = U_0 = 5E_s$ correspond to equilibrium distribution, which is taken as a rectangle with width $\delta U_0 = 0.0434E_s$ (the interval for breaking up U in numerical calculations).

It is clear from Fig. 1 that in the absence of extraneous gas, toward the middle of the pumping pulse ($t/t_0 = -0.2$) there is a considerable increase in the average vibrational energy of the assemblage of molecules both in the ground state and in the excited state. In the absence of stimulated emission (Fig. 1a, b) this increase is smaller and corresponds to an increase of the temperature $T_0 = 580$ K to an average temperature $\bar{T} = \bar{U}/(kN)$ equal to $\bar{T} = 660$ K for the ground and excited states. The process of increasing vibrational temperature in the system is limited to the region of U where the quantum yield of fluorescence $q(U) = p_{21}/p_2(U)$ is still fairly high (Fig. 1, curve 5) since the process of depletion of populations of the system accelerates with increasing U. Under lasing conditions (Fig. 1c, d) the radiative lifetime of level 2 decreases and the effective value of q increases, and therefore the system may be heated to higher average temperatures $\bar{T} = 810$ K. In the absence of neutral gas, distributions n_1 and n_2 under lasing conditions show narrow peaks with a width of the order of that of the lasing spectrum. These peaks under lasing conditions are due to the fact that some of the molecules acquire a reserve vibrational energy equal to $-E_{se} \approx E_s/2$ (since $E_p = 0$) in every cycle of absorption and stimulated emission; as a result, the narrow peak of equilibrium distribution is transformed to peaks with higher U, spaced with an interval of approximately $-E_{se}$ with respect to the reserve vibrational energy. The broad distribution of n_1 and n_2 with respect to U is determined by the process of spontaneous emission, where a molecule in each cycle of absorption and emission may change its reserve of vibrational energy by any amount within the limits of the width of the fluorescence spectrum. All curves

in Fig. 1 except curves 1 of Fig. 1a, b are normalized to the maximum value. The latter consist of a broad part and a sharp peak at $U \approx U_0$ with a value that exceeds the maximum in the broad part of the distribution by a factor of 9.1 (Fig. 1a) and 8.5 (Fig. 1b) times. However, the areas of the segments of distribution 1 that correspond to this peak are smaller than the areas under the broad part of the curve by a factor of about 4, and therefore curves 1 in Fig. 1a and b are normalized to maxima that correspond to the broad part of the distribution; the narrow peak of distribution 1 on Fig. 1a, b is not marked.

As the number of collisions with the neutral gas (pressure P) increases, the quantity $\bar{U}$ becomes smaller, and the distribution itself narrows. In the absence of stimulated emission, the distributions $n_1(U)$ and $n_2(U)$ get close to the equilibrium distributions at $pt_0 > 200$ ($P \sim 5$ atm) and the system approaches a solution in its characteristics. Under conditions of stimulated emission, due to shortening of the lifetime of level 2, an active molecule undergoes more acts of absorption and emission, and therefore deviations of the distributions $n_1(U)$ and $n_2(U)$ from the equilibrium distribution are observed at higher neutral gas pressures. Collisional redistribution of energy also leads to disappearance of the narrow peaks on the curves for distribution of $n_1(U)$ and $n_2(U)$ under lasing conditions. The presence of extraneous gas also considerably slows down the process of depletion of the population of the system. For example the complete normalized populations of level 1 $n_1/n_0 = \int n_1(U)\, dU/n_0$ in the absence of lasing are equal to 0.131, 0.198 and 0.203 at P = 0, 5 and 25 atm, and under lasing conditions for the same values of P, $n_1/n_0 = 0.0095$, 0.69 and 0.79 respectively.

The process of increasing vibrational energy in the pre-lasing period has its effect on the lasing threshold f_0^{th}, which may increase considerably (as compared with the f_0^{th} in solutions) due to depletion of the population of the system and an increase of losses in channel $1 \to 2$ on λ_{se}. Obviously this increase will be the more appreciable the greater the duration of the pumping pulse front or the value of E_p; it will also be considerable for low-Q cavities. Shown in Fig. 2a is the dependence of f_0^{th} on the losses of Q in the cavity for different neutral gas pressures. It can be seen that at fairly large Q (6-8) the value of f_0^{th} in the absence of a stabilizing gas is several times greater than the corresponding value at a high extraneous gas pressure ($P \sim 100$ atm). For the chosen

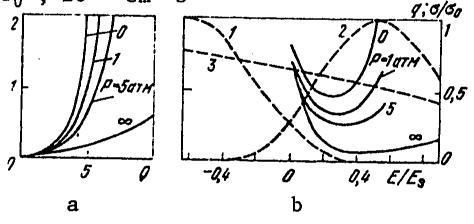

Fig. 2. Dependence of lasing threshold f_0^{th} on Q at $E_p = E_s/2$ (a) and on E_p at Q = 5 (b); spectra of amplification σ_{21} (1) and absorption σ_{12} (2), and $q(E/E_s)$ (3)

values of the parameters in the calculation, the increase in f_0^{th} is almost entirely due to depletion of the two-level system in the pre-lasing period. Consideration of large values of Q in the calculation is justified by the fact that we have disregarded accumulated losses that are inevitable when working with vapor.

In the case of solutions, for the selected conditions of uniform circulation and low losses on λ_{se} in channel $1 \to 2$, the optimum pumping wavelength λ_p^{opt} at which the threshold is minimum, is equal in accordance with the maximum rate of excitation to the wavelength of the maximum of the absorption band ($E_p^{opt} = E_s/2$). For vapor the quantity f_0^{th} also depends on the rate of heating of the system in the pre-lasing period, and therefore λ_p^{opt} in this case is shifted into the region of the long-wave slope of the absorption band ($E_p^{opt} < E_s/2$), where the rate of heating is slower. Curves of the dependence of f_0^{th} on E_p are shown in Fig. 2b. When losses are fairly high in the resonator ($Q = 5$), the λ_p^{opt} for rarefied vapor is appreciably shifted into the long-wave region; in this case $f_0^{th}(E_p^{opt})$ for the vapor is considerably greater than the corresponding value for a solution (curve ∞).

The harmful effect that heating in the system has on lasing intensity and efficiency, in contrast to its influence on the threshold, may show up in the case of low losses in the optical cavity and low values of E_p. An increase in the rate of growth of reserve vibrational energy under lasing conditions involves an increase in cycles of absorption and emission per unit of time. The behavior of lasing efficiency for vapor (the ratio of the integral number of emission quanta during a pulse to the number of pumping quanta absorbed in the active layer) is shown in Fig. 3 (curve 1). Since no forms of induced absorption are present, the lasing efficiency depends but little on the extraneous gas pressure. Curve 2 of Fig. 3 corresponds to the pressure dependence of the number of quanta W of stimulated emission extracted from the cavity during a lasing pulse. It can be seen that with an increase in pressure from 0 to 25 atm, the quantity W increases by a factor of about 6. The poor lasing characteristics at $P = 0$ are due to the rapid increase of $\bar{U}$ during stimulated emission, which leads to depletion of working levels 1 and 2, and to disruption of lasing. As the losses in the system and the duration of the pumping front increase, there is a rapid reduction of W in rarefied vapor. As the neutral gas pressure increases, there is an increase in the duration and intensity of stimulated emission. At pressure $P = 25$ atm ($pt_0 = 1000$) all molecules of levels 1 and 2 are concentrated in the region of values of U that are

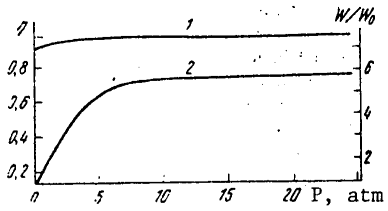

Fig. 3. Dependence of lasing efficiency η (1) and the integral number of quanta of stimulated emission W (2) on neutral gas pressure P

close to the equilibrium value, where the probability that molecules will leave the system of levels 1 and 2 is low, which leads to values of W that are close to the corresponding values in a liquid. The reduction in lasing efficiency at low P is also related to the increase of K_{th} in the spectral region of stimulated emission caused by the increase in σ_{12} on λ_{se} in connection with increasing U.

The change of $\bar{U}$ during lasing may have a considerable effect on formation of the lasing spectrum and change of wavelength λ_{se}^{max} at the intensity maximum. The results of numerical calculation of stimulated emission in vapor for different neutral gas pressures are shown in Fig. 4. The process of change in the lasing spectrum (spectral width $\Delta\lambda_{se}$, λ_{se}^{max}) in time is illustrated by diagrams consisting of families of lines of equal intensity with coordinates of time t/t_0 plotted against lasing wavelength λ (or E). The distance between lines of equal intensity is $\Delta\gamma(t,E) = 7.5/(E_s\sigma_0)$. As can be seen from Fig. 4a, in the absence of extraneous gas λ_{se}^{max} (curve 1) is shifted appreciably during lasing toward the long-wave side (by approximately 3 nm). As the neutral gas pressure increases this shift decreases and at P = 25 atm there is almost no shift of the lasing line with time. In the latter case the process of development of stimulated emission in vapor is practically no different from that in the liquid phase.

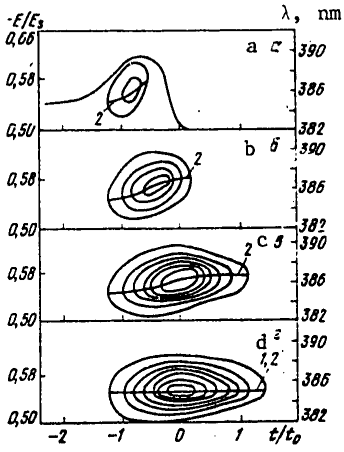

Fig. 4. Diagrams of formation of the lasing spectrum at P = 0 (a), 2 (b), 5 (c) and 25 (d) atm, and time dependences of λ_{se}^{max} (2) and λ_0^{max} (1)

The long-wave displacement of λ_{se}^{max} takes place due to an increase in the overlap of spectra of amplification and absorption because of increasing U during lasing. Curve 1 (Fig. 4a) shows the behavior of the wavelength λ_0^{max} (or E_0^{max}) of the maximum total gain $K_\gamma - K_\Pi$ in the system in a time interval wider than the lasing duration. The long-wave shift of λ_0^{max} has the same cause, i. e. an increase in K_Π with increasing $\bar{U}$, as the corresponding shift of λ_{se}^{max}. As time passes, the populations of levels 1 and 2 are strongly depleted, the concentration of excited molecules falls, and K_Π decreases, approaching zero throughout the lasing spectrum. Under these conditions, the long-wave shift of λ_0^{max} is replaced by a short-wave shift, λ_{se}^{max} being gradually displaced into the region of the maximum of $\sigma_{21}(E)$. However, by the time that the short-wave shift of λ_0^{max} has shown up, lasing has practically stopped, and therefore the short-wave displacement of λ_{se}^{max} goes unobserved. The difference between λ_0^{max} and λ_{se}^{max} reflects a considerable lag in the change of λ_{se} with a change in lasing conditions. At P ~ 25 atm the vibrational energy of the system remains practically unchanged (at the

assumed value of U_0, the depletion of system of levels 1 and 2 is also small), which is what makes λ_0^{max} and λ_{se}^{max} constant, and consequently equal throughout the lasing region (Fig. 4d).

Thus the results of the theoretical analysis done in this paper show that even in the most favorable case of absence of induced absorption, the lasing characteristics of organic compounds in vapors are poorer than in solutions. In the presence of induced absorption on the lasing and pumping wavelengths, the difference between lasing characteristics of vapors and solutions increases still more in favor of the latter.

REFERENCES

1. N. A. Borisevich, I. I. Kalosha, V. A. Tolkachev, ZHURNAL PRIKLADNOY SPEKTROSKOPII, Vol 19, 1973, p 1108.

2. N. A. Borisevich, A. Ya. Gorelenko, V. A. Povedaylo, V. A. Tolkachev, ZHURNAL PRIKLADNOY SPEKTROSKOPII, Vol 25, 1976, p 332.

3. B. Steyer, F. P. Schäfer, APPL. PHYS., Vol 7, 1975, p 113.

4. N. A. Borisevich, A. Ya. Gorelenko, I. I. Kalosha, V. A. Povedaylo, V. A. Tolkachev, ZHURNAL PRIKLADNOY SPEKTROSKOPII, Vol 28, 1978, p 906.

5. G. A. Abakumov, Yu. M. Anisimov, B. I. Polyakov, A. P. Simonov, KVANTOVAYA ELEKTRONIKA, Vol 6, 1979, p 397.

6. V. P. Klochkov, V. L. Bogdanov, B. S. Neporent, PIS'MA V ZHURNAL EKSPERIMENTAL'NOY I TEORETICHESKOY FIZIKI Vol 13, 1971, p 47.

7. P. W. Smith, F. P. Liao, C. V. Shank, T. K. Gustafson, C. Lin, P. J. Maloney, IEEE J., QE-11, 84, 1975.

8. N. A. Borisevich, L. N. Bolot'ko, V. A. Tolkachev, DOKLADY AKADEMII NAUK SSSR, Vol 218, 1974, p 320.

9. V. S. Zuyev, Yu. Yu. Stoylov, K. K. Trusov, ZHURNAL PRIKLADNOY SPEKTROSKOPII, Vol 23, 1975, p 1003.

10. V. S. Zuyev, Yu. Yu. Stoylov, K. K. Trusov, KVANTOVAYA ELEKTRONIKA, Vol 4, 1977, p 443.

11. S. V. Davydov, Candidate's Dissertation, Minsk 1978.

12. V. V. Gruzinskiy, S. V. Davydov, ZHURNAL PRIKLADNOY SPEKTROSKOPII, Vol 29, 1978, p 231.

13. N. A. Borisevich, "Vozbuzhdennyye sostoyaniya slozhnykh molekul v gazovoy faze" [Excited States of Complex Molecules in the Gas Phase], Minsk: Nauka i tekhnika, 1976.

14. Yu. T. Mazurenko, IZVESTIYA AKADEMII NAUK SSSR: SERIYA FIZIKA, Vol 39, 1975, p 2299.

15. B. S. Neporent, ZHURNAL FIZICHESKOY KHIMII, Vol 13, 1939, p 983.

6610
CSO: 1862

UDC 621.373.826.038.823

A MULTIBEAM WAVEGUIDE CO_2 LASER WITH AC DISCHARGE EXCITATION

Moscow KVANTOVAYA ELEKTRONIKA in Russian Vol 7, No 2(92), Feb 80
pp 425-429 manuscript received 28 Aug 79

[Article by V. V. Antyukhov, A. F. Glova, O. R. Kachurin and F. V. Lebedev, Institute of Atomic Energy imeni I. V. Kurchatov, Moscow]

[Text] 1. The interest recently noted in studying steady-state waveguide CO_2 lasers is due to the high specific characteristics of these devices [Ref. 1], as well as to the possibility of tuning the emission frequency over a range of several gigahertz [Ref. 2], which opens up prospects for putting them to practical use in communications, radar, molecular spectroscopy and so on. Attainment of high absolute values of output power is such lasers is limited by technical difficulties that arise in setting up long discharge capillaries, and cannot be realized without sacrificing compactness of the device. The outlook for increasing the output power of waveguide lasers (WL) opens up with a design described in Ref. 3, consisting of a parallel arrangement of gas-discharge tubes with common mirrors. With this design, the authors of Ref. 3 were able to make a compact laser with power of about 3 kW, opening up ways to use the WL for technological purposes.

Since the limiting power invested per unit of length of the discharge tube of a laser with diffusion cooling is independent of its diameter, a further increase in laser power without increasing dimensions is possible as a result of reduction of the diameter of the discharge tubes. However, when a DC discharge is used for laser pumping [Ref. 1-4], reducing the diameter of discharge tubes and increasing their number runs up against technical difficulties due to the necessity for putting a large number of high-voltage electrodes into the tubes and providing for commutation of these electrodes. These difficulties can be completely overcome by using a capacitive AC discharge to pump the working medium. This arrangement can be the basis of a simple, compact electrodeless design of a multibeam laser, enabling an increase in overall efficiency by eliminating energy losses in the active ballast resistances.

Despite intensive development of WL equipment, up until now there have been no unambiguous results that enable prediction of optimum working conditions for these devices. The large number of variable parameters and the necessity of accounting for a process as poorly investigated as quenching of vibrationally excited molecules on the walls of the tube result in uncertainty in numerical calculations of gain K_0 [Ref. 5-7]. The measured values of K_0 are strongly dependent on the specific conditions of the experiment (cooling conditions, material of the gas discharge tube, composition of the mixture, rate of circulation and so on), and are different for different authors (see for example Ref. 7, 8). Numerical calculations and measurements of saturation intensity I_s made under analogous conditions differ by a factor of about two [Ref. 6, 9].

Pumping the medium by an AC discharge makes prediction of the optimum working conditions of the laser still more difficult, and is accompanied by modulation of the output power. This leads to the necessity for experimental investigation of the effectiveness of the proposed method of excitation.

This paper for the first time gives the results of an investigation of the optical properties of the active medium of a waveguide CO_2 laser pumped by a low-frequency AC discharge, and also discusses the characteristics of the output emission of a multibeam laser with the proposed excitation technique.

2. A diagram of the experimental facility is shown in Fig. 1,a. A steady capacitive discharge with frequency from 10 to 70 kHz is set up in interchangeable tubes 1 immersed in cell 2 with circulating coolant 3. The

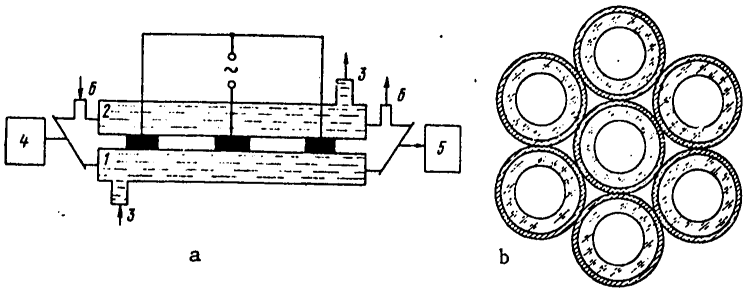

Fig. 1. Diagram of experimental facility (a), and cross section of an assembly of seven tubes (b)

electrodeless discharge tubes 25 cm long were made of molybdenum glass with wall thickness of about 1 mm. Tube diameters were 1.3, 2.5 and 5.5 mm. The working mixture 6 (CO_2:N_2:He = 1:1:3 and 1:1:6) was circulated at a static pressure on the tube inlet of 5-120 mm Hg at a rate of 1-10 m/s. The weak-signal gain averaged over the cross section of the tube was measured by stabilized diagnostic laser 4.

The output characteristics of the multibeam waveguide CO_2 laser excited by AC discharge were studied on an uncooled assembly consisting of seven parallel tubes with inside diameter of 2.5 mm and length of 25 cm (Fig. 1,b). The laser cavity was made up of two flat mirrors: an opaque copper mirror and an uncoated gremanium mirror placed at the ends of the assembly. The outside diameter of the assembly was 17 mm. The laser operated in the quasi-steady state with pulse duration of about 10 ms. The fluctuations of emission output power were registered by Ge-Au photocell 5.

3. The gain of the active medium K_0 and the output characteristics of the laser depended on the average discharge current <I>, the pressure p of the mixture and the frequency f of the discharge current. Variation of the circulation rate within the given range corresponding to the diffusion cooling mode had practically no effect on the experimental results.

With increasing $\langle I\rangle = 2f\int_0^{1/2f} |I|\,dt$ (where I is the instantaneous value of the discharge current, the values of K_0 and the output power W of the laser passed through a maximum. The optimum currents $\langle I_0\rangle$ corresponding to maximum W were practically independent of the pressure of the mixture, and amounted to about 8 mA at p = 20 mm Hg, about 10-11 mA at p ≈ 30-40 mm Hg, and 7-8 mA at p ≈ 70-80 mm Hg.

Typical curves for the maximum K_0 and w = W/L as functions of p are given in Fig. 2. The dependence of K_0 on tube diameter d is illustrated by Fig. 3. Shown in Fig. 4 are experimental curves for the depth of modulation of laser output emission δW/W as a function of <I>, p and f. The

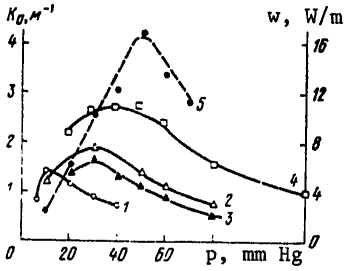

Fig. 2. Curves for maximum gain of the medium (1-4) and specific output power w (5) as a function of the pressure of the working medium for mixtures of CO_2:N_2:He = 1:1:3 (1, 3, 4) and 1:1:6 (2, 5) at f = 10 (1) and 70 (2-5) kHz, d = 5.5 (1), 2.5 (2, 3, 5) and 1.3 (4) mm, <I> = 8 mA

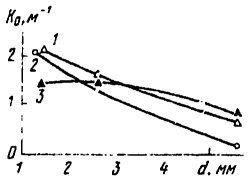

Fig. 3. Gain of the medium K_0 as a function of discharge tube diameter for mixtures of CO_2:N_2:He = 1:1:3 (1, 2) and 1:1:6 (3) at f = 70 kHz, $\langle j\rangle$ = 100 mA/cm^2, p = 20 (1, 3) and 40 (2) mm Hg

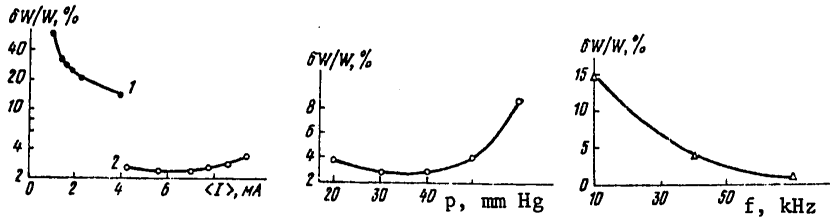

a b c

Fig. 4. Dependence of the depth of modulation of laser output radiation on the average discharge current <I> (a), the pressure of the mixture (b) and frequency of the discharge current (c): a) p = 40 mm Hg, f = 10 kHz (1) and 40 kHz (2); b) <I> = 9 mA, f = 40 kHz; c) p = 40 mm Hg, <I> = 4 mA

maximum values of K_0 attained in our experiments were 1.5, 2.3 and 3.2 m^{-1} for tube diameters of 5.5, 2.5 and 1.3 mm respectively. The total emission power of the laser reached 30 W, which corresponds to a specific power extracted from a unit of length of each tube w ~ 17 W/m. The maximum values of the specific volumetric energy input <jE> were ~40 W/cm^2.

4. Let us compare the experimental results with the waveguide laser characteristics that are available in the literature.

If we use the relations found for $K_0(p)$ and the literature data on the saturation parameter $I_s(p)$ [Ref. 9], the maximum output power under our conditions should be expected at $p \approx 50$–60 mm Hg, which agrees with the curve for W(p) in Fig. 2.

The expected relation $K_0(d) \sim d^{-1}$ [Ref. 2] in the case of absence of relaxation of molecules on the wall was satisfied in our experiments only for a mixture of CO_2:N_2:He = 1:1:3 at p = 40 mm Hg. At lower pressures, as can be seen from the curves of Fig. 3, K_0 increases with decreasing d for the same mixture more slowly, while for a mixture of CO_2:N_2:He = 1:1:6 the optimum K_0 is observed at $d \approx 2.5$ mm. Such behavior of the curves for $K_0(d)$ in all probability is due to accelerated relaxation of the vibrationally excited molecules on the walls of the tube because of reduced diffusion time with helium enrichment of the mixture and reduction of p [Ref. 10].

A distinguishing feature of a laser excited by an AC discharge is modulation of the output radiation caused by the periodic energy release in the discharge and excitation of particles [Ref. 11]. Using the expression for output radiation power of Ref. 12

$$W = {}^1/_2 I_s \theta \{[K_0 L/(\varkappa+\theta)]-1\} S_{\text{эф}}, \qquad (1)$$

where I_s is saturation intensity, θ is transparency of the cavity, $\varkappa$ is the intracavity losses, the depth of modulation can be approsimated as

$$\delta W/W \approx L K_0/[2f\tau_p(K_0 L-\varkappa-\theta)], \qquad (2)$$

where τ_p is the effective time of relaxation of vibrational energy of the molecules. The resultant relation explains the nature of the experimental dependences of $\delta W/W$ on $\langle I \rangle$, p and f shown in Fig. 4.

With laser operation far from the emission threshold ($K_0 L >> \kappa + \theta$), $\delta W/W$ does not depend on current, and hence is independent of pumping intensity as well. The weak increase in $\delta W/W$ at $\langle I \rangle \gtrsim 8$ mA can probably be attributed to a reduction of τ_p due to the increase in temperature of the mixture. As the emission threshold is approached, $K_0 L - \kappa - \theta$ approaches zero, and $\delta W/W$ should increase in the limit to 100%. This is just the behavior of curve 1 in Fig. 4a obtained close to the threshold. The discontinuity between curves 1 and 2 is due to change in frequency of the discharge current.

The increase in $\delta W/W$ at $p > 40$ mm Hg (see Fig. 4b) is due to a reduction in $\tau_p \sim 1/p$, and also a reduction in K_0. The increase in $\delta W/W$ in the low-pressure region ($p \lesssim 30$ mm Hg) is caused in all probability by a reduction in the effective relaxation time due to additional quenching of vibrationally excited particles on the walls of the discharge tube.

As was to be expected, $\delta W/W$ decreases with increasing f (see Fig. 4c), and at f = 70 kHz, p = 40 mm Hg and $\langle I \rangle = 4$ mA, $\delta W/W$ does not exceed 1-1.5%. An estimate of $\delta W/W$ by formula (2) with the use of data on the rate of collisional relaxation taken from Ref. 13 gives $\delta W/W \approx 1.5\%$. The presence of output modulation with frequency 2f is no barrier to the use of a multibeam laser in technology. Moreover, the possibility of varying $\delta W/W$ over a wide range (from 1 to 100%) may be of independent interest.

5. Let us compare the output characteristics of the WLs with different excitation techniques. The maximum emission power from a unit of active length of a BeO discharge tube at d = 2.55 mm and total discharge length L = 94 mm was achieved in Ref. 1, and comes to $w \approx 41$ W/m at overall emission power of $W \approx 4$ W and specific volumetric energy input $jE \approx 90$ W/cc. The limiting values of w attainable for the optimum cavity according to the authors of Ref. 1 are ~46 W/m. The maximum output power of ~3 kW was attained in a multibeam WL 4 m long consisting of ~40 tubes with diameter d ~ 1 cm and overall diameter of the assembly ~25 cm [Ref. 3]. The value of jE in this case did not exceed ~2 W/cc, and $w \approx 20$ W/m.

The values of $w \approx 17$ W/m measured in our experiments were obtained under conditions of non-optimum cavity transparency, and according to our estiamtes, as well as data of Ref. 8, they can be increased by 2-3 times. The achievement of lasing on an assembly of seven tubes 2.5 mm in diameter excited by an AC discharge demonstrated the fundamental feasibility of appreciably reducing the overall dimensions of powerful multibeam lasers. Even at the already attainable values of w, a laser with power of 1 kW at a length of ~1 m can be made from a set of about 50 tubes with diameter of 2.5 mm with outside diameter of about 50 mm for the assembly. The use of an AC discharge eliminates the major technical

problems that would have to be solved if such a laser were excited by a DC discharge.

6. The given experimental investigations have shown the feasibility of effective use of a low-frequency AC discharge (10-70 kHz) for pumping waveguide CO_2 lasers. The actual laser has high specific characteristics and is simple to make. The use of electrodeless discharge tubes enables construction of a simple and compact multibeam laser with high overall emission power. Such a laser may find wide application in technological processes such as laser heat-hardening of alloys.

In conclusion the authors thank V. S. Golubev for useful discussions, V. N. Litvinov and S. S. Barsukov for assistance in preparation of the experiment.

REFERENCES

1. D. R. Hall, R. M. Jenkins, E. E. Gorton, P. H. Cross, J. PHYS. D., Vol 10, 1977, p 1.

2. A. S. Provorov, V. P. Chebotayev, in: "Gazovyye lazery" [Gas Lasers], Novosibirsk: Nauka, 1977.

3. G. I. Kozlob, V. A. Masyukov, V. A. Kuznetsov, PIS'MA V ZHURNAL TEKHNICHESKOY FIZIKI, Vol 4, 1978, p 129.

4. J. J. Degnan, APPL. PHYS., Vol 11, 1966, p 1.

5. A. M. Sinitsyn, KVANTOVAYA ELEKTRONIKA, Vol 5, 1978, p 2179.

6. H. Shirahata, S. Nakao, JAPAN. J. APPL. PHYS., Vol 17, 1978, p 1255.

7. B. A. Kuzyakov, KVANTOVAYA ELEKTRONIKA, Vol 6, 1979, p 114.

8. E. G. Burkhardt, T. J. Bridges, P. W. Smith, OPTICS COMMS., Vol 6, 1972, p 193.

9. K. Matsumoto, H. Shirahata, T. Fujioka, IEEE, QE-14, 1978, p 781.

10. T. J. Bridges, E. G. Burkhardt, P. W. Smith, APPL. PHYS. LETTS., Vol 20, 1972, p 403.

11. V. D. Gavrilyuk, A. F. Glova, A. B. Kuznetsov, F. V. Lebedev, V. A. Feofilaktov, KVANTOVAYA ELEKTRONIKA, Vol 6, 1979, p 548.

12. A. V. Yeletskiy, B. M. Smirnov, "Gazovyye lazery," Moscow: Atomizdat, 1971.

13. R. Taylor, S. Witterman, REV. MOD. PHYS., Vol 41, 1969, p 26

6610
CSO: 1862

UDC 621.373.826

INTENSITY FLUCTUATIONS OF THERMALLY SELF-STRESSED LASER RADIATION IN A TURBULENT MEDIUM

Moscow KVANTOVAYA ELEKTRONIKA in Russian Vol 7 No 3 (93), 1980 pp 545-552
manuscript received 24 Jul 79

[Article by B. S. Agrovskiy, V. V. Vorob'yev, A. S. Gurvich, V. V. Pokasov and A. N. Ushakov, Institute of Atmospheric Physics of the USSR Academy of Sciences, Moscow]

[Text] The spatial spectra of the intensity fluctuations of laser radiation passing through an absorbing turbulent medium are studied theoretically and experimentally. It is shown that in the case of propagation of spatially coherent radiation, thermal nonlinearity leads at first to attenuation, and then to amplification of the intensity fluctuations. The degradation of coherency leads to a reduction of both the relative fluctuations in the intensity and nonlinear effects.

The experimental detection of the effect of the attenuation of intensity fluctuations of CW laser radiation in the case of its thermal self-stress on itself in a turbulent medium was reported in paper [1]. This effect is qualitatively explained by the appearance of thermal defocusing lenses in the focusing regions by random inhomogeneities and focusing lenses in regions with light intensities less than the average. However, correct calculations of the variation in the fluctuations in the case of continuous radiation have not been successfully performed, something which is due to the difficulties in accounting for turbulent intermixing.

The attenuation effect in intensity fluctuations, as follows from a qualitative treatment, should also manifest itself in the case of propagation of laser pulses of sufficiently high energy in a turbulent absorbing medium. In this case, if the pulse width τ is much less than the characteristic times for the variation in the turbulent inhomogeneities, one can consider the problem of radiation propagation in a stationary medium. The results of the calculations given in this paper show that attenuation of intensity fluctuations of spatially coherent radiation is possible in this case in a limited range of pulse energy

densities. In the case of energy densities W which are greater than a certain level W_k (which depends on the path length L and the dimensions of the inhomogeneities l_0), the relative fluctuations in the intensity increase with an increase in the energy.

The question of the influence of fluctuations of the spatial coherency of the radiation incident to the medium is discussed. It is well known that in the absence of self-stress, radiation incoherency also leads to attenuation of intensity fluctuations [2], though in a nonlinear medium, as was indicated in paper [3], incoherency can lead to a reduction in the influence of nonlinearity on the change in the spatial spectrum of the fluctuations. Based on the representation of the laser radiation field as a field produced by a remote thermal source of finite angular dimensions, estimates are made of the influence of incoherency on the fluctuations.

Measurements of the spatial spectra of intensity fluctuations of multimode pulsed radiation in a turbulent medium have shown the substantial attenuation of fluctuations due to thermal self-stress. Experimental results are in good agreement with the results of calculations which take into account the incoherency of the radiation.

1. The Calculation of Weak Fluctuations in the Intensity of Pulsed Radiation

We shall describe the propagation of radiation in an absorbing medium with large scale inhomogeneities, neglecting molecular thermal conductivity, by the equations

$$2ik\frac{\partial E}{\partial z}+\Delta_\perp E+k^2\left(\frac{1}{\varepsilon_0}\frac{\partial \varepsilon}{\partial T}T+\frac{\varepsilon_1}{\varepsilon_0}\right)E=0; \tag{1}$$

$$T=\frac{\alpha c\exp(-\alpha z)}{8\pi\rho c_p}\int_0^t |E|^2\,dt, \tag{2}$$

where k is the wave number; c is the speed of light in a vacuum; ε_0 is the average dielectric permittivity of the medium; ε_1 (x, y, z) is the fluctuation component of the dielectric permittivity; T is the change in the temperature of the medium during radiation absorption; α, ρ and c_p are the absorption factor, density and heat capacity of the medium respectively.

In the absence of turbulence ($\varepsilon_1 = 0$), the system of equations (1) and (2) permits a solution in the form of a plane wave:

$$E_0=A_0\exp[i\varphi_0(t,z)];\quad \varphi_0=\frac{k}{2\varepsilon_0}\frac{\partial \varepsilon}{\partial T}\frac{J_0 t\,[1-\exp(-\alpha z)]}{\rho c_p}, \tag{3}$$

where $J_0=\alpha c A_0^2/8\pi$ is the radiation power density. The plane wave approximation is applicable if one can neglect the divergence of the beam due to diffraction and thermal defocusing, i.e., when the following conditions are met: $z \ll ka^2$, $z \ll \left(-\frac{2}{\pi\varepsilon_0}\frac{\partial\varepsilon}{\partial T}\frac{\alpha W}{\rho c_p a^4}\right)^{-1/2}$, where a is the half-width of the beams; $W = \pi a^2 J_0 t$ is the pulse energy. If the fluctuations in the dielectric permittivity ε_1 and the fluctuations they cause in the intensity are small, to calculate the field fluctuations one make use the method of smooth perturbations. By representing the function E in the form $E = A_0\exp(i\phi_0 + \chi + i\phi)$, given the condition $\chi \ll 1$, we obtain the following equations for the function χ and ϕ:

$$2k\frac{\partial\chi}{\partial z} + \Delta_\perp\varphi = 0; \tag{4}$$

$$2k\frac{\partial\varphi}{\partial z} - \Delta_\perp\chi - \frac{2k^2\alpha J_0 e^{-\alpha z}}{\varepsilon_0\rho c_p}\frac{\partial\varepsilon}{\partial T}\int_0^t \chi(x,y,z,t')\,dt' = \frac{\varkappa^2}{4\varepsilon_0}\varepsilon_1(\rho, z). \tag{5}$$

It is convenient to solve this system of equations using the Fourier transform method with respect to the transverse coordinates x and y. For the spectral components: $\chi(\varkappa) = \frac{1}{(2\pi)^2}\iint \chi(\rho, z)\exp(-i\varkappa\rho)\,d^2\rho$

we obtain the equation:

$$\chi'' + \frac{\varkappa^4}{4k^2}\chi + \varkappa^2 q^2 e^{-\alpha z}\frac{1}{\tau}\int_0^t \chi(\varkappa, z, t')\,dt' = \frac{\varkappa^2}{4\varepsilon_0}\varepsilon_1(\varkappa, z), \tag{6}$$

where $q = \left(-\frac{2}{\varepsilon_0}\frac{\partial\varepsilon}{\partial T}\frac{\alpha J_0\tau}{\rho c_p}\right)^{1/2}$

Having in mind the interpretation of experimental observations in a laboratory model of a turbulent medium, the length of which L is less than the characteristic diffraction length $L_d = 2d/\kappa^2$, we shall limit ourselves to calculations of the fluctuations in an approximation of geometric optics. Moreover, we shall neglect the attenuation of the radiation energy due to absorption. Given these assumptions, the applicability of which will be discussed later, equation (6) is written in the form:

$$\chi'' + \varkappa^2 q^2\frac{1}{\tau}\int_0^t \chi(\varkappa, z, t')\,dt' = \frac{\varkappa^2}{4\varepsilon_0}\varepsilon_1(\varkappa, z). \tag{7}$$

We shall initially treat the solutions of the homogeneous equation corresponding to (7). These solutions can be written in the form of a series:

$$u_1(z,t) = \sum_{n=0}^{\infty} c_n\xi^{2n}; \quad u_2(z,t) = z\sum_{n=0}^{\infty} d_n\xi^{2n},$$

where $\xi = z/L_T$ is a dimensionless coordinate; $L_T = L_\varkappa = \left(\varkappa q\sqrt{\frac{t}{\tau}}\right)^{-1}$ is

the characteristic thermal self-stress length; the coefficients c_n and d_n are determined by the recurrence formulas:

$$c_n = -\frac{c_{n-1}}{2n^2(2n-1)}; \quad d_n = -\frac{d_{n-1}}{2n^2(2n+1)}; \quad d_0 = c_0 = 1. \tag{8}$$

In the case of small values of ξ, we have the following for the functions u_1 and u_2:

$$u_1 = 1 - \frac{1}{2}\xi^2 + \frac{1}{48}\xi^4 + \ldots, \quad u_2 = z\left(1 - \frac{1}{6}\xi^2 + \frac{1}{240}\xi^4 + \ldots\right), \tag{9}$$

from which it can be seen that both the amplitude and phase initial perturbations of the incident wave will initially be suppressed (when $\xi \leq 1$) by the thermal nonlinearity.

The asymptotes of the functions u_1 and u_2 when $\xi >> 1$, as can be shown by substitution in equation (7), will be as follows:

$$\begin{aligned} u_1 &\sim A_1\xi^{-1/3}\exp(a\xi^{2/3}) + \ + \text{complex conjugate} \\ u_2 &\sim A_2 z\xi^{-1}\exp(a\xi^{2/3}) + \\ &\qquad + \text{complex conjugate} \end{aligned} \tag{10}$$

where $a = 3\cdot 2^{-5/3}(1+i\sqrt{3})$; ; A_1 and A_2 are complex coefficients.

Thus, at large distances in a medium ($z >> L_T$), the initial perturbations are amplified. This is due to the fact that the spatial modulation of the intensity at the input to the nonlinear medium leads to time modulation in the depth of the medium. The characteristic modulation period τ_m and its frequency $\Omega \simeq \tau_m^{-1}$ at a distance z in the medium can be estimated from the condition $L_T(\tau_m) = z$, from which $\Omega \simeq \kappa^2 q^2 z^2/\tau$. However, in the presence of space-time modulation of the intensity, for example, of the form $\chi(\rho, t) = \chi(\rho)\cos\Omega t$, the sign of the temperature perturbations of the medium

$$T \sim \qquad T \backsim \int_0^t \chi dt = \chi(\rho)\sin\Omega t/\Omega$$

can be opposite to the sign of the intensity perturbations. For this reason, self-focusing and amplification of the perturbations are possible.

We shall find the solution of the nonhomogeneous equation (7), just as the homogeneous one, by using a series expansion in powers of t:

$$\chi(\varkappa, z, t) = \sum_{n=0}^{\infty} r_n(z)\, t^n. \tag{11}$$

Then we have the following equations for r_n:

$$\dot{r_n} = -\frac{\varkappa^2 q^2}{\tau}\,\frac{r_{n-1}}{n}, \quad \dot{r_0} = -\frac{\varkappa^2}{4\varepsilon_0}\,\varepsilon_1(\varkappa, z) \tag{12}$$

with the boundary conditions $r(0) = r_n'(0) = 0$. The solution of equations (12) can be written in the form:

$$r_n = -\frac{\varkappa^2}{4\varepsilon_0}(-1)^n\left(\frac{\varkappa^2 q^2}{\tau}\right)^n \frac{1}{n!\,(2n+1)!}\int_0^z (z-z')^{2n+1}\varepsilon_1(\varkappa, z')\,dz'.$$

We shall designate the sum of the following series as g(t, z-z'):

$$g(t, z-z') = \sum_{n=0}^{\infty} (-1)^n \left(\frac{\varkappa^2 q^2 t}{\tau}\right)^n \frac{1}{n!\,(2n+1)!}\,(z-z')^{2n+1}, \qquad (13)$$

and then:

$$\chi(\varkappa, z, t) = -\frac{\varkappa^2}{4\varepsilon_0}\int_0^z g(\varkappa, z- \\ -z', t)\,\varepsilon_1(\varkappa, z')\,dz'.$$

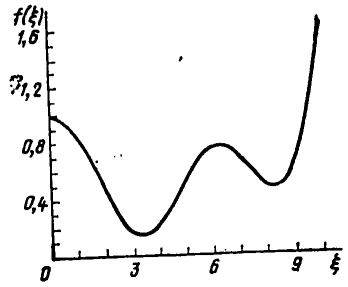

Figure 1. A graph of the function f(ξ) defined by expressions (15).

To simplify the calculations of the fluctuation spectrum χ, we shall assume that the fluctuations ε_1 are delta correlated with respect to z:

$$\langle \varepsilon_1(\varkappa_1, z_1)\,\varepsilon_1^*(\varkappa_2, z_2)\rangle = 2\pi\Phi_\varepsilon(\varkappa)\delta(\varkappa_1 - \\ -\varkappa_2)\delta(z_1-z_2), \text{ where } \langle \chi(\varkappa_1, z, t)\,\chi^*(\varkappa_2, \\ z, t)\rangle = \Phi_\chi(\varkappa)\delta(\varkappa_1-\varkappa_2), \text{ where}$$

$$\Phi_\chi(\varkappa, z, t) = \frac{\pi\varkappa^4}{24\varepsilon_0^2}\,z^3\Phi_\varepsilon(\varkappa)\,f(\varkappa, z, t); \qquad (14)$$

$$f(\varkappa, z, t) = \sum_{n=0}^{\infty} \frac{3}{2n+3}\,b_n\xi^{2n};\ b_n = \sum_{k=0}^{n} d_k d_{n-k};\ \xi = \varkappa q z\sqrt{t/\tau}; \qquad (15)$$

The coefficients d_k are defined by formula (8). The graph of the function f(ξ), which characterizes the influence of the thermal nonlinearity on the fluctuation spectrum of the logarithm of the amplitude, is shown in Figure 1. A clear presentation of the change in the fluctuation spectrum of the log of the amplitude Φ_χ and the dispersion $\langle\chi^2\rangle$ in a turbulent medium with an ε_1 fluctuation spectrum of the form

$$\Phi_\varepsilon(\varkappa) = C\varkappa^{-11/3}\exp(-\varkappa^2/\varkappa_m^2) \qquad (16)$$

are shown in Figures 2 and 3. The parameter which characterizes the influence of the nonlinearity in this case will be:

$$\xi_0 = \varkappa_m q z\sqrt{t/\tau}. \qquad (17)$$

As can be seen from Figures 1 - 3, thermal nonlinearity leads to the suppression of the high frequency portion of the spectrum and a reduction in the dispersion of $\langle\chi^2\rangle$ when $\xi_0 \lesssim 3.5$. However, with a further increase in the parameter ξ_0, the fluctuations increase. We shall recall that these

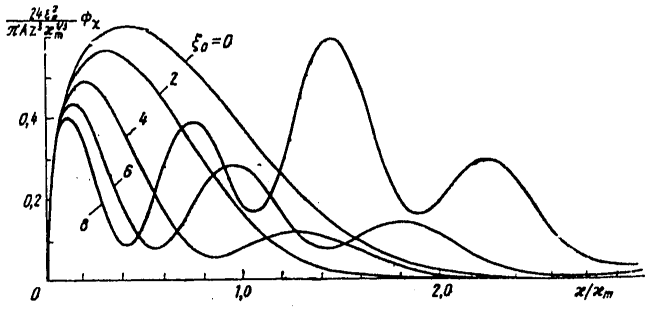

Figure 2. The variation in the Φ_χ fluctuation spectrum in the case of thermal self-action.

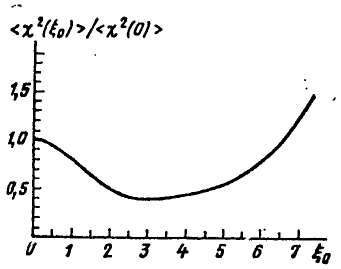

Figure 3. The change in the dispersion of the intensity fluctuations in the case of self-action.

conclusions are justified in the case of weak fluctuations $\langle\chi^2(\xi_0)\rangle \ll 1$, $\langle\chi^2(\xi_0)\rangle = Q\langle\chi^2(0)\rangle$,

where $\langle\chi^2(0)\rangle = (\pi^2\varkappa_m^{4/3}/24\varepsilon_0^2)\, C\Gamma(5/6)z^3$ is the dispersion of the fluctuations χ in the absence of nonlinearity; $Q(\xi_0)$ is a function, the graph of which is shown in Figure 3.

2. The Influence of Diffraction, the Attenuation of Radiation Energy and Its Incoherency on the Fluctuations

Estimates of the influence of diffraction and attenuation of the energy due to absorption can be based on calculations of the spectrum of the initial perturbations in a homogeneous nonlinear medium. The results of calculations of the change in the spectrum of fluctuations χ in a nonlinear medium are shown in Figure 4, where the spectrum at the input had the form $\Phi_\chi(0) = \exp(-\kappa^2/\kappa_m^2)$, taking into account both the diffraction characterized by the parameter $D = \kappa_m^2 z/2k$, and the absorption for the case $\xi_0 = 3.3$, which corresponds to the maximum attenuation of the fluctuations (when $D = 0$, $\alpha z \ll 1$) and the values of the parameters $D = 0.5$ and $\alpha z = 1$, which are close

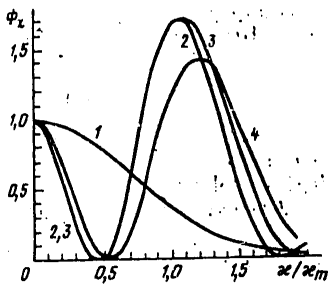

Figure 4. The influence of diffraction and attenuation of the beam energy due to absorption at the ϕ_χ fluctuation spectrum where $\xi_0 = 0$ (a linear medium) (1); $\xi_0 = 3.3$, $\alpha z = 0$, $D = 0$ (geometric optics) (2); $\xi_0 = 3.3$, $\alpha z = 0$, $D = 0.5$ (3) and $\xi_0 = 3.3$, $\alpha z = 1$, $D = 0$ (4).

to those realized in the experiment. It can be seen from a comparison with calculations using the approximation of geometric optics that both diffraction and attenuation do little to change the spectrum of the fluctuations χ, at least in the range of wave numbers of $\kappa/\kappa_m \geq 2$.

The incoherency of the radiation proves to be more important. Correctly accounting for the multimodality of the radiation is quite complicated and we shall limit ourselves here to qualitative estimates. We shall first consider the fluctuations in the absence of self-stress. We shall characterize the degree of radiation coherence by the coherence radius r_k, which can be determined from the beam divergence angle θ: $r_k = \lambda/\theta$.

The distribution of the field produced by a remote thermal source of finite angular dimensions can serve as a model of distribution of the partially coherent light field at the boundary of a turbulent medium. The coherency radius of the field produced by such a source in the Fraunhofer diffraction region is likewise determined by the ratio $r_k = 1.22\,\lambda/\theta$, where θ is the angular dimension of the source (for example, see [4]). The method of calculating the intensity fluctuations of the light wave of remote thermal sources of finite dimensions is given in book [5]. By using this method, it is not difficult to derive the following expression for the dispersion of the light intensity fluctuations in the range of applicability of geometric optics ($D \leq 1$) and in the case where the turbulence spectrum is specified by formula (16):

$$\langle \chi^2 \rangle = \iint \Phi_\chi(\varkappa, \theta, z)\, d^2\varkappa = \langle \chi^2(\theta = 0, z) \rangle 3 \int_0^1 \xi^2 [1 + (\theta z \varkappa_m \xi/2)^2]^{-7/6} d\xi, \qquad (18)$$

where

$$\Phi_\chi = \frac{\pi}{24} \frac{z^3}{\varepsilon_0^2} \varkappa^4 \Phi_\varepsilon(\varkappa)\, \varphi\left(\frac{\varkappa \theta z}{2}\right) \qquad (19)$$

is the spectrum of the fluctuations of the logarithm of the amplitude of the partially coherent source. The influence of incoherency is taken into

account by the function:

$$\varphi(y) = 3\int_0^1 \xi^2 \exp(-y^2\xi^2)\, d\xi. \qquad (20)$$

The approximation of the function H(x) from [5] of the form H(x) = $= \exp(-x^2/8)$ was used in deriving formulas (18)-(20).

For the cases of small and large values of the angle θ, we find from (18):

$$\langle\chi^2\rangle = \frac{\pi^2}{24}\frac{C}{\varepsilon_0^2}\Gamma\left(\frac{7}{6}\right)\varkappa_m^{7/3}z^3\left[1+\frac{7}{10}\left(\frac{\varkappa_m\theta z}{2}\right)^2\right] \text{ при } \varkappa_m\theta z \ll 1;$$

$$\langle\chi^2\rangle = \frac{3\pi^2}{16}\frac{C}{\varepsilon_0^2}\Gamma\left(\frac{7}{6}\right)\left(\frac{\theta z}{2}\right)^{-7/3}z^3 \text{ при } \varkappa_m\theta z \gg 1. \qquad (21)$$

As can be seen from the last formula, the radiation intensity fluctuations of an incoherent source increase with distance more slowly than the fluctations in a plane wave, in which case, they do not depend on χ_m. The attenuation of the fluctuations is explained by the fact that at any point at a distance z in a turbulent medium, the intensity is the sum of the intensities of plane waves arriving at this point from the region of the medium bounded by a cone with an aperture angle of θ. As a result, the small scale spikes in the intensity are averaged in a manner similar to the averaging of the fluctuations of the light flux by an objective of radius $l = \theta z$. Only overshoots with dimensions on the order of l lead to intensity fluctuations in this case.

The formula for the fluctuations of $\langle\chi^2\rangle$ in the case of partially coherent radiation can be derived from formula (20) for a plane wave, by substituting $(\theta z)^{-1}$ for $\varkappa_m$ in it. It will agree with formula (21) with a precision of down to a constant factor.

Similar arguments can also be adduced for estimates of the influence of incoherency on the self-stress effect. In accordance with them, the quantity $\varkappa_m$ in the expression for the parameter ξ_0 (17), which characterizes the influence of nonlinearity, should be replaced by $(\theta z)^{-1}$. The influence of nonlinearity will then be determined by the quantity:

$$\xi_{\theta\phi} = \eta q\sqrt{l/\tau}/\theta, \qquad (22)$$

where η is a coefficient on the order of unity.

3. Experimental Results

The spatial structure of a pulsed laser beam after it passed through an absorbing turbulent medium was studied experimentally. A GOR-300 laser generated multimode radiation in a pulse with a width of about 8 msec. The pulse energy was monitored with an IKT-1M meter and varied in a range of

30 - 120 J. The beam diameter at the input to the turbulent medium was 2 cm and the angular divergence of the beam was 10^{-2} rad. The beam passed through a cell with ethyl alcohol which was dyed with methylene blue to produce the monitored absorption α. Flat heat exchangers were placed at the upper and lower boundaries of the liquid to produce convective turbulence. The results given below were obtained with the following parameters: the absorption coefficient was $\alpha = 0.04$ cm^{-1}; the temperature of the upper and lower boundaries of the liquid was 52 and 14° C respectively; the spacing between the heat exchangers was 4.5 cm. The values of C and κ_m in formula (16) can be estimated in accordance with [6]: $C = 5.4 \cdot 10^{-8}$ cm$^{-2/3}$ and $\kappa_m = 57$ cm^{-1}. The distribution of the intensity at the rear wall of the cell was photographed with an SKS-2 camera at a rate of about 4,000 frames/sec using MZ-2 motion picture film.

The photographs were computer processed for quantitative studies of the change in the intensity fluctuations. The distribution of the light intensity $J_{k,l} = J(x_k, y_l)$ at the corners of a grid with dimensions of $b/(m-1)$, where $b = 1.32$ cm is the width of a side of the square located in the center of the beam; $m = 128$ is the number of subdivision points along each axis, was computed taking into account the charateristic density curve for the film. Two-dimensional spectra of the intensity fluctuations were computed using a fast Fourier transform:

$$\Phi_i(p, q) = |c_{p,q}|^2, \quad c_{p,q} = \frac{4}{m^2} \sum_{k,l=0}^{m-1} J_{k,l} \exp\left[i \frac{2\pi}{m} (kp + lq)\right] \tag{23}$$

as well as one-dimensional spectra of the relative fluctuations in the intensity:

$$\tilde{F}_i(p) = 2 \sum_{q=0}^{m/2-1} \Phi_i(p, q)/c_{0,0}^2. \tag{24}$$

Examples of experimental one-dimensional intensity fluctuation spectra $\tilde{F}_i$, which illustrate their timewise evolution are shown in Figure 5. Also depicted here are theoretical curves for $F_i(\kappa/\kappa_m, \xi_{э\phi})$ [$\xi_{э\phi} = \xi_{eff}$], computed from the two-dimensional spectra of Φ_χ taking into account the isotropicity of the fluctuations:

$$F_i(\varkappa/\varkappa_m, \xi_{э\phi}) = 4\varkappa_m \int_{-\infty}^{\infty} \Phi_\chi\left[\sqrt{\varkappa^2/\varkappa_m^2 + t^2}, \xi_{э\phi}\right] dt.$$

For convenience in making a comparison with experimental values, a dimensionless spectrum F_i was introduced so that the dispersion of the relative intensity fluctuations was $\beta^2 = 4\langle\chi^2\rangle = \int F_i(\varkappa/\varkappa_m) d(\varkappa/\varkappa_m)$. In order to take into account the influence of both the radiation incoherency and the thermal nonlinearity, the Φ_χ spectrum was chosen as follows in accordance with formulas (14), (19) and (22):

$$\Phi_\chi = \frac{\pi}{24\varepsilon_0^2} z^3 \Phi_\varepsilon(\varkappa) \varkappa^4 f(\xi_{э\phi}) \varphi\left(\frac{\varkappa\theta z}{2}\right). \tag{25}$$

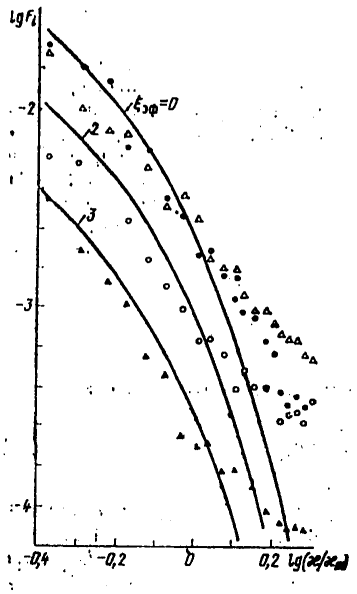

Figure 5.

The change in the one-dimensional intensity fluctuation spectra with time.

The solid lines are computed from Formula (27) where B = 280; the dots are experimental values where W = 23 (solid black dots), 100 J (triangles, light circles, black triangles) and t/τ = 1/27 (black dots), 1/35 (light triangles), 2/5 (circles with a dot in the center) and 31/35 (black triangles).

The function ϕ, defined by expression (20), can be approximated by the following expression with an error of no more than 5%:

$$\varphi(y)=(1+4y^3/3\sqrt{\pi})^{-1}. \tag{26}$$

Taking into account the values of the parameters C and κ_m, we derive the following expression for the spectrum F_i (when z = 25 cm):

$$F_i\left(\frac{\kappa}{\kappa_m},\ \xi_{э\phi}\right)=1{,}6f(\xi_{э\phi})\int_{-\infty}^{\infty} y^{1/6}e^{-y}(1+By^{3/2})^{-1}dr, \tag{27}$$

where $y=\kappa^2/\kappa_m^2+r^2$; $B=(4/3\sqrt{\pi})(\kappa_m\theta z/2)^2$. . The theoretical curves shown in Figure 5 were computed for the case of V = 280, which corresponds to θ = = 10 mrad.

When $200 \leq B \leq 300$ and $0.4 \leq \kappa/\kappa_m \leq 2$, $\log F_i$ as a function of B can be approximately described by the formula:

$$\lg F_i(B, \kappa/\kappa_m)=\lg F_i(250, \kappa/\kappa_m)-2{,}5\cdot 10^{-3}(B-250).$$

Curves corresponding to $\xi_{э\phi}$ = 0, 2 and 3 are shown in Figure 5. The values of these parameters for the experimental curves were computed from the formula:

$$\xi_{э\phi}(t)=\frac{\eta}{\theta}\sqrt{-\frac{2}{\varepsilon_0}\frac{\partial\varepsilon}{\partial T}\frac{\alpha\overline{W}t}{\pi a^2\rho c_p\tau}}$$

where W = 100 J, α = 0.04 cm^{-1}, a = 1 cm, and will be $\xi_{eff} = 1.77\eta$ for the 14th frame (t/τ = 14/35) and $\xi_{eff} = 2.64\eta$ for the 31st frame. A comparison

of the experimental curves with the theoretical ones makes it possible to specify the value of the undetermined coefficient η more precisely.

When $\eta = 1.1$, good agreement is observed between the theoretical and experimental spectra in a range of wave numbers of $0.4 \leq \kappa/\kappa_m \leq 1.3$. However, there is no such agreement outside of this range, something which is related to the influence of the boundedness of the beam on the low frequency portion of the spectrum ($\kappa/\kappa_m < 0.4$), and apparently, to the difference between the turbulent spectrum $\phi_\varepsilon(\kappa)$ and the spectrum specified by formula (16) in the region of high frequencies ($\kappa/\kappa_m > 1.3$). As can be seen from Figure 5, in the absence of self-stress, the experimental spectra of F_i when $\kappa/\kappa_m \approx 2$ fall off more slowly than $\exp(-\kappa^2/\kappa_m^2)$, as follows in the case of the function ϕ_ε in the form of (16). It is desirable to perform an experiment using a coherent source in order to come to more definite conclusions concerning the behavior of the spectrum in the high frequency region.

The authors are grateful to V.P. Trusov for assisting in the performance of the experiment.

BIBLIOGRAPHY

1. B.S. Agrovskiy, et al., KVANTOVAYA ELEKTRONIKA [QUANTUM ELECTRONICS], 7, 59, (1980). [sic]

2. M.I. Mordukhovich, IZV. VUZOV. SER. RADIOFIZIKA [PROCEEDINGS OF THE HIGHER EDUCATIONAL INSTITUTES, SERIES ON RADIOPHYSICS], 13, 275, 1970.

3. G.A. Pasmanik, ZhETF [JOURNAL OF EXPERIMENTAL AND THEORETICAL PHYSICS], 66, 490, (1974).

4. D. Klauder, E. Sudarshan, "Osnovy kvantoboy optiki" ["The Principles of Quantum Optics"], Moscow, Mir Publishers, 1970, p 36.

5. A.S. Burvich, A.I. Kon, V.L. Mironov, S.S. Khmelevtsov, "Lazernoye izlucheniye v atmosfere" ["Laser Radiation in the Atmosphere"], Moscow, Nauka Publishers, 1976, p 227.

6. A.S. Gurvich, M.A. Kallistratova, F.E. Martvel', IZV. VUZOV. SER. RADIOFIZIKA, 20, 1020, (1977).

8225
CSO: 1862

UDC 621.373.826.038.823

A STUDY OF THE CHARACTERISTICS OF PHOTOIONIZATION EXCIMER LASERS

Moscow KVANTOVAYA ELEKTRONIKA in Russian Vol 7 No 3 (93), 1980 pp 593-598
manuscript received 24 Aug 79

[Article by V.M. Borisov, F.I. Vysikaylo, S.G. Mamonov, A.P. Napartovich and Yu.Yu. Stepanov]

[Text] The results of experimental and theoretical studies of the characteristics of photoionization excimer lasers as a function of the preionization conditions, the charging voltage and the partial composition of the gaseous mixture are given. Optimal conditions for laser operation are found, under which the lasing energy for the KrF molecule amounted to one Joule.

The possibility of easily and efficiently producing a volumetric discharge with the free ionization of gas by ultraviolet radiation has generated interest in studying its electrical and lasing characteristics. In particular, it was established in paper [1] that there exists a threshold concentration of photoelectrons for TEA CO_2 lasers, which when reached, the discharge acquires a volumetric character. A further increase in the photoelectron concentration in a wide range by virtue of the increase in the energy contributed to the auxiliary discharge did not change the discharge and lasing characteristics. The presence of a significant amount of halogens (0.1 - 1%) in the working mixtures of excimer lasers substantially changes the governing laws related to preionization which apply to CO_2 lasers. A study of the efficiency of XeF and KrF lasers as a function of the free ionization delay time with respect to the primary discharge was carried out in papers [2, 3]. The functions which were obtained are explained by the presence of fluorine in the working gas mixture. A power supply circuit including an LC oscillator [4] or a Blumline line is used in almost all electrical discharge excimer lasers known at the present time, while preionization is accomplished by one row of sparks positioned on the side and along the center of the interelectrode gap. The typical lasing energy obtained in such lasers amounts to 0.1 J. The laser described in paper [6] is an exception. The authors

of this work obtained an energy of 0.8 J using a complex system of energy repumping and discharge voltages of 140 KV; in this case, the efficiency of the laser amounted to about 0.1 percent. It should be noted that such high charging voltages are extremely inconvenient for the design of lasers operating in a frequency mode.

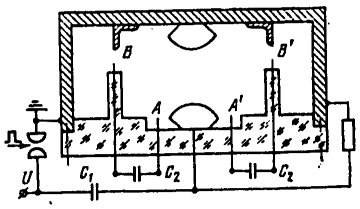

Figure 1. A schematic of the experimental setup.

The results of experimental and theoretical studies of the characteristics of photoionization excimer lasers are given in this work as a function of the preionization conditions, charging voltage and partial composition of the gas mixture. Optimum conditions are found for laser operation, under which the lasing energy for the KrF molecule amounted to 1 J. A schematic of the experimental setup in shown in Figure 1. The metal housing of the chamber is grounded, the cover is made of plexiglass, and four rows of metal rods 5 mm in diameter are placed in it, with 11 rods in each row. The discharge electrodes are fabricated from aluminum bar stock 40 mm in diameter and 60 cm long; the interelectrode spacing is 5 cm. A KMK-100-0.06 capacitor with a capacitance of 0.06 μFd was used as C_1; C_2 was built up with KVI-3 capacitors, so that the capacity of a single element was 150 pf, while the equivalent capacitance of all of the elements of one row was 1,650 pf. The resonator was formed by a fully enclosed aluminum reflector and a plane-parallel plate made of CaF_2. When C_1 is switched, pulse charging of C_2 takes place, and in this case, two series of sparks (A and A') occur close

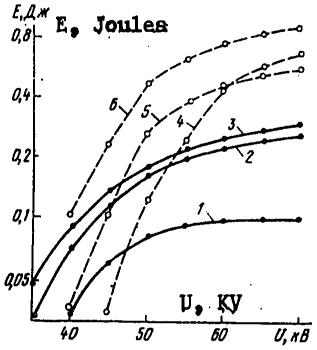

Figure 2.

The XeF (solid line) and KrF (dashed line) lasing energies as a function of the voltage for various preionization levels.

Key: 1, 4. Illumination only by the B and B' rows of sparks;
2, 5. Only by the A and A' rows of sparks;
3, 6. Total illumination.

to the high voltage electrode and two series (B and B') on both sides of the discharge gap. The ultraviolet radiation of the sparks produces the preionization of the gas volume.

We measured the lasing energy and simultaneously recorded the oscilloscope voltage and current traces when various rows of sparks were covered with shields opaque to UV radiation. The results of measurements of the XeF and KrF lasing energies are shown in Figure 2 as a function of the charging voltage and the illumination geometry. The dependence of the lasing energy on the geometry of the UV preionization for the XeCl molecule is very close to similar functions for XeF. It can be seen from Figure 2 that preionization by only the sparks of rows A and A' is more effective as a rule than preionization by the sparks of only rows B and B'. This can be explained by the generation of a lower concentration of photoelectrons in the working volume by virtue of the greater distance of spark rows B and B' from the discharge gap. The utilization of the illumination from all the rows of sparks leads to an even greater increase in the lasing energy. It can also be seen from Figure 2 that preionization yields the strongest effect in the case of low charging voltages (30 - 40 KV).

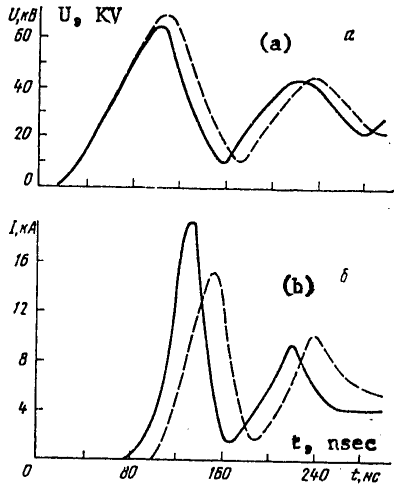

Figure 3.

The computed oscilloscope traces of the voltage (a) and current (b) in the case of high (solid line) and an order of magnitude lower (dashed line) preionization level.

Thus, in contrast to the well-known laser designs [1 - 6], where preionization was realized by a set of sparks powered from an individual capacitor and located to the side of the discharge at a spacing of 4 to 6 cm, we have shown that the preionizer sparks must approach the discharge gap in a manner similar to A and A'. It is important to underscore the fact that it is specifically the production of powerful homogeneous preionization which has made it possible to use a simple discharge supply circuit configuration with one switcher, in contrast to the previously used circuits [4, 5]. In such a circuit configuration (see Figure 1), a type TGI-2500/50 thyratron, operating at a voltage of 35-50 KV can be used in place of the discharger, and a pulse-periodic laser operating mode is realized. The circuit we used for this operation likewise has the advantage that preionization is accomplished automatically, without a second switcher.

The computed oscilloscope current and voltage traces are shown in Figure 3, in which case, the current is of an oscillating nature with a sharply pronounced first peak. An analysis of the oscilloscope traces shows that the energy contribution to the discharge over the time of the first current peak amounts to about 50 percent of the total stored in the capacitors. Since the contribution to the discharge following the first current peak is realized at low values of the parameter E/N (as compared to its value at the maximum of the first current peak), the excitation of the lower resonance and metastable levels of Xe and Kr [7] becomes ineffectual, and for this reason, from the viewpoint of laser efficiency only the energy contribution in the first current peak is important. In the following, we shall understand the words "energy contribution to the discharge" to mean the energy contribution in the first current peak and will designate it as $\mathcal{E}$.

It was found from the experimental oscilloscope traces of the voltage and current that $\mathcal{E}$ increases with an increase in the charging voltage, as well as with the introduction of halogens (0.2 percent) into the pure helium and does not change substantially with a change in the preionization level. Thus, the increase in the lasing energy observed with an increase in the preionization level (see Figures 2, 3) cannot be explained by the change in the energy contribution to the bulk discharge.

The current and voltage oscilloscope traces were calculated using a homogeneous discharge model in a manner similar to [7] to explain the observed functions. The equations which describe the main elementary processes in this case have the form:

$$\frac{dn_e}{dt} = \nu_i^* n_{\mathrm{He}}^* + \nu_i n_e + K_{ic} n_{\mathrm{Kr}}^* n_e - \nu_a n_e + q; \tag{1}$$

$$\frac{dn_{\mathrm{He}}^*}{dt} = \nu_B^* n_e - \nu_i^* n_{\mathrm{He}}^* - K_i (n_{\mathrm{He}}^*)^2; \tag{2}$$

$$\frac{dn_{\mathrm{Kr}}^*}{dt} = \nu_B n_e - K_{ic} n_{\mathrm{Kr}}^* n_e - \nu_T n_{\mathrm{Kr}}^*, \tag{3}$$

where n_e is the electron concentration; n_{He}^* and n_{Kr}^* are the concentrations of He and Kr atoms in the metastable states; ν_i^* is the Penning ionization frequency of the easily ionizing molecules and atoms by the helium atoms in the metastable states; ν_i is the frequency of direct ionization of He, F_2 and Kr by electron impact; ν_a is the frequency of dissociative adhesion of electrons of to F_2 molecules; ν_B^* and ν_B are the excitation frequencies of the helium and krypton atoms respectively to metastable states; q takes into account the formation of photoelectrons due to ultraviolet preionization; K_{ic} is the ionization rate constant for Kr atoms in metastable states due to electron impact; ν_T is the extinction rate of krypton atoms in metastable states by heavy particles; K_i is the Penning ionization rate constant for the case of collision of two helium atoms

in metastable states. The Penning ionization rate constant of F_2 molecules and Kr atoms was chosen as $K_i \approx 10^{-10}$ cm^3/sec, just as for nitrogen [8]. The remaining ionization and excitation rate constants due to electron impact were selected in accordance with paper [7]. (We will note the closeness of the results of the calculations of the various constants in papers [7] and [9].)

As a result of calculations using the model described here, pretty good agreement was achieved between the experimental and calculated voltage and current oscilloscope traces.

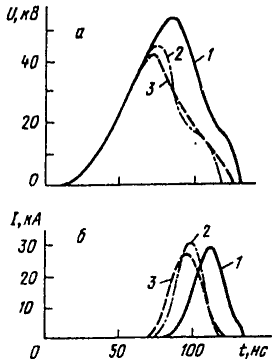

Figure 4. Oscilloscope traces of the current and voltage computed for the following mixtures:
F_2:He = 0.2:99.8 (1);
F_2:He:Kr = 0.2:94.8:5 (2); and for pure He (3);
U_0 = 50 KV and p = 1.5 atm.

The increase in ε when fluorine is added to the helium ($\leq$ 0.2%) can be explained by the increase in the breakdown voltage which is due to the acceleration of electron extinction due to their adhesion to F_2 and the reduction in the ionization rate due to the decrease in the tail of the electron distribution function, as well as by the increase in the maximum value of the current due to the growth in the ionization when the Penning reaction of He with F_2 starts. At significant concentrations of fluorine ($\geq$ 1%), electrons are formed primarily by virtue of direct ionization of the fluorine. The oscilloscope traces of the voltage and current in this case take on a sharply pronounced oscillatory character, and flashover is visually observed in the form of several bright channels against the background of the diffuse discharge.

The results of a numerical calculation of the voltage and current oscilloscope traces at a pressure of 1.5 atm and a charging voltage of U_0 = 50 KV for various mixtures are shown in Figure 4 by way of illustration. The energy contribution to the discharge in pure He amounted to $\mathcal{E}$ = 38 J/l. With the addition of 0.2% F_2, the energy contribution increased up to $\mathcal{E}$ = = 53 J/l, and with the addition of Kr to the lasing mixture, it fell off to 44 J/l.

An increase in the preionization level, as calculations have shown, leads to a somewhat greater growth in the concentration of metastable He atoms

with respect to the increase in the concentration of electrons. The delay in the generation of electrons because of the Penning reaction leads to a slight increase in the current in the first peak. However, this effect is small. It can be seen from Figure 3 that an increase by a factor of 10 in the preionization level leads only to a 20% increase in the energy contribution, something which is in agreement with experimental results.

The analysis of the numerical calculation of a discharge in an He-F_2 mixture made it possible to ascertain four stages in the development of a discharge, each of which is described in a simplified fashion. Ionization due to the ultraviolet source predominates in the first stage, ionization due to the Penning reaction with metastable He predominates in the second, direct ionization of He and F_2 in the third, and in the fourth stage, stepwise ionization proves to be the primary form.

We shall write simplified expressions for $n_e(t)$ and $n^*_{He}(t)$ in each of the stages:

$$1.\ n_e = q/\nu_a,\ n^*_{He} \approx \int_0^t q\nu^*_B/\nu_a dt;$$

$$2.\ n_e \approx n_{e1} \exp\left[\int^t \left(\sqrt{\nu^*_B \nu_a} - \nu_i\right) dt\right],\ n^*_{He} \approx \sqrt{\nu^*_B/\nu^*_i}\ \sqrt{n_e^2 - C_2^2};$$

$$3.\ n_e \approx n_{e2} \exp\left[\int^t (\nu_i - \nu_a)\, dt\right],\ n^*_{He} \approx \frac{\nu^*_B}{\nu^*_i} n_e + C_3\ ;$$

$$4.\ n_e \approx K_{ic} n_e \left(\frac{\nu^*_B}{\nu_i} n_e + C_4\right).$$

Here n_{e1}, n_{e2}, C_2, C_3 and C_4 are constants which can be found from the conditions of blending the solutions.

The possibility of the breakdown into the indicated stages is determined both by the conditions in the discharge network and by the gas composition. When the conditions change, the duration of the individual stages changes as well as the parts they play in the overall current rise. Subsequently, the fourth stage is replaced, obviously, by a current reduction stage which is related to the drop in the voltage. The same type of breakdown into stages is also observed for laser mixtures (with the addition of Kr, Xe). We will note that in the first three stages, the growth in n_e is proportional to the original concentration, while there is a peaking in the fourth stage which is related to stepwise ionization. It was assumed in accordance with the estimates that the recombination is low in all stages. Under these conditions, steady-state burning of the discharge is unstable [10]. Both the experiment and the

Table

U_0, KV	E, J	I, KA	E/N, T_d	$\frac{n_{e0}}{n_{eM0}}$	$\frac{n_{e1}}{n_{eM1}}$	Explanations
50	15.4	25.3	23	1/2	85	The basic calculation.
50	14.9	27.8	20.7	10/20	122	n_{e1} and n_{e0} increased by a factor of 10.
50	15.3	27.7	22.8	1/2	76.3	The following reactions are considered: $He^* + Kr \rightarrow e$ and $H^* + F_2 \rightarrow e$.
50	14.8	27.4	22.1	1/2	39	The reaction rate constants for $He^* + Kr \rightarrow e$ and $He^* + F_2 \rightarrow e$ were increased by a factor of 10.
70	21.6	40.7	24.4	1/2	64.6	The following reactions are considered: $He^* + Kr \rightarrow e$, $He^* + F_2 \rightarrow e$.

Note: U_0 is the charging voltage; n_{e0} and n_{eM0} are the initial and maximum electron concentrations in the main discharge; n_{e1} and n_{eM1} are the same in the segregated current column.

calculations demonstrated that the growth in laser power with an increase in the ultraviolet illumination power is not related to an increase in the energy contribution to the discharge. To study the influence of the inhomogeneity in the preionization level, we shall modify the discharge model, segregating from the whole homogeneous volume that column with an initial concentration which differs from the mean value. We shall likewise assume that the dimensions of the column are small enough that its contribution to the overall current is small, and for this reason, the field is determined by the main volume of the discharge.

As follows from the preceding analysis, the initial difference in the concentrations can be increased only in the fourth stage, something which is a manifestation of instability [10]. Numerical calculations have shown that under the conditions of the discharge, there occurs amplification of the initial overshoot of the electron concentration by a factor of 50 to 100 (Table). It has been noted that with an increase in the charging voltage, the amplification of an inhomogeneity falls. This correlates with the experimentally observable increase in discharge stability with a rise in the charging voltage. In the general case, discharge stability is improved when the contribution of the fourth stage to its development is reduced.

Thus, calculations show that the equalization of the ultraviolet preionization level promotes the development of a more homogeneous discharge, something which should have a positive effect on the lasing characteristics.

BIBLIOGRAPHY

1. V.M. Borisov, Yu.A. Satov, V.V. Sudakov, KVANTOVAYA ELEKTRONIKA [QUANTUM ELECTRONICS], 3, 2460, (1976).

2. R.P. Akins, G. Innis, Shao-Clu Lin, J. APPL. PHYS., 49, 2262, (1978).

3. J. Hsia, APPL. PHYS. LETTS., 30, 101, (1977).

4. R. Burnham, N. Djeu, APPL. PHYS. LETTS., 29, 707, (1976).

5. I.M. Isakov, A.G. Leonov, V.Ye. Ogluzdin, PIS'MA V ZhTF [JOURNAL OF TECHNICAL PHYSICS], 4, 1228, (1978).

6. R.S. Taylor, W.J. Sarjeant, A.J. Alcock, K.E. Leopold, OPTICS COMMS., 25, 231, (1978).

7. V.Yu. Baranov, et al., Preprinty IAE [Institute of Nuclear Power Preprints] Nos. 3080 and 3081, Moscow, 1979.

8. F.W. Lee, C.B. Collins, J. CHEM. PHYS., 65, 5189, (1976).

9. A.E. Greene, C.A. Brau, IEEE J. QE-14, 951, (1978).

10. J.B. Daugherty, J.A. Mangano, J.H. Jacob, APPL. PHYS. LETTS., 28, 581, (1976).

8225
CSO: 1862

UDC 533.92

THE CHANGE IN THE ENERGY CHARACTERISTICS OF AN ELECTROIONIZATION DISCHARGE IN MIXTURES OF CO_2-N_2-He AND COMMERCIAL GRADE NITROGEN DURING PULSE PERIODIC OPERATION

Moscow KVANTOVAYA ELEKTRONIKA in Russian Vol 7 No 3 (93), 1980 pp 630-633
manuscript received 28 Aug 79

[Article by Ye.P. Glotov, V.A. Danilychev, V.D. Zvorykin, Yu.S. Leonov, A.M. Soroka and N.V. Cheburkin, Physics Institute imeni P.N. Lebedev of USSR Academy of Sciences, Moscow]

[Text] The effect of the change in the characteristics of an electroionization discharge is studied in mixtures of CO_2-N_2-He and commercial grade nitrogen for the case of pulse periodic operation of an electrical ionization laser. It is found that when $E/p \leq 5$ KV/(cm·atm) and with specific energy inputs which do not exceed 500 J/(l·atm), the change in the discharge characteristics of the indicated mixtures of CO_2-N_2-He and commercial grade nitrogen is determined only by the action of the electron beam. The drop in the energy contribution is related to the formation of oxides of nitrogen as a result of plasma chemical reactions, where the molecules of the nitrogen oxides possess very high electron adhesion rate constants ($\approx 10^{-10}$ cm^3/s).

When designing CW and quasicontinuous closed cycle [1] electrical ionization lasers (EIL) with repeat use of the lasing mixture, one of the most important problems is that of mixture degradation, since it is specifically this process which determines the gas consumption during the operation of a CO_2 laser in pulse-periodic and CW modes. This paper is devoted to an investigation of the discharge characteristics of the lasing mixture of [2] during pulse-periodic operation of an EIL.

The experiments were performed using a laser installation with an active volume of 10 liters, which was described in paper [3]. The ionization of the medium was accomplished by an electron beam with a current density of $j_e \approx 0.5$ A/cm^2 and a pulse width of $\tau = 1.5$ microseconds, which was generated by an electron gun with a point cathode. The high voltage pulses were

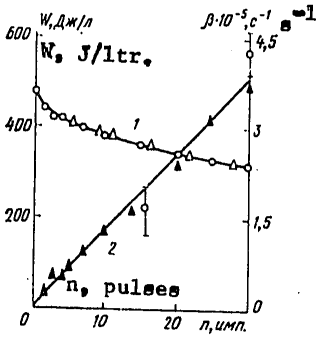

Figure 1. The specific energy contribution in commercial grade nitrogen (light circles), electron beam current without discharge (light triangles) and the adhesion rate constant β (dark triangles) as a function of the number of preceding discharge current pulses, n. The light circles with short horizontal lines above and below them correspond to the values of β computed from the results of mass spectrometer measurements of the concentrations of the nitrogen oxides formed in the discharge.

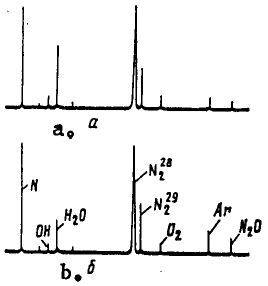

Figure 2. Mass spectrograms of commercial grade nitrogen before (a) and after (b) 30 energy contribution pulses.

generated by a Marx generator with impulse capacitance of 0.04 μfd. The discharge current was measured by a Rogowski loop, operating in the RC integration mode (R = 300 ohms, C = 0.05 μfd).

In the course of the experiment, mass spectrometer studies of the composition of the gas mixture were performed as a function of the number of energy contribution pulses, as a result of which it was established that in an electrical ionization discharge in mixtures of CO_2-N, cyanogen CN and hydrocyanic acid HCN are formed, which in being electronegative, can increase the effective electron adhesion rate. Following 30 discharge pulses, which corresponds to an overall energy contribution averaged over the entire volume of the laser cell (a passive volume of 200 liters) of 0.5 KJ/l, and 0.06% CN and 0.03% HCN were formed in a mixture of CO_2:N_2 = 1:5. However, as further experiments demonstrated, the formation of cyanogen and hydrocyanic acid is not the main reason for the reduction in the energy contribution to electrical ionization discharge, since the electron adhesion rate increases not only in mixtures of CO_2 - N_2, but also in commercial grade nitrogen where CN and HCN can, in principle, not be produced. The energy contributed to the discharge is shown in Figure 1 as a function of the number of preceding pulses for commercial grade nitrogen with an oxygen content of 0.4%.

In order to determine what contribution is made by the electron gun in the absence of discharge to the formation of electronegative additives, the energy W introduced into the discharge was recorded as the function of the number of preceding electron gun pulses without discharge, which agreed (see Figure 1) with the curve for the energy contribution as a function of the number of discharge current pulses. This makes it possible to draw the conclusion that the formation of electronegative impurities in an electrical ionization discharge in a range of field intensities of $E/p \leq 5$ KW/(cm · atm) and the energy contributions W = 200--500 J/(l · atm) is determined only by the action of the electron gun on the gas mixture.

A mass spectrometer analysis showed that as a result of the action of the electron gun, the oxygen content in commercial grade nitrogen is reduced, and a peak with a mass number of 44 appears in the mass spectrogram, which corresponds to nitrous oxide N_2O. Characteristic mass spectrograms for commercial nitrogen before (a) and after (b) 30 energy contribution pulses are shown in Figure 2.

It is well known that molecules of the nirogen oxides N_2O and NO_2 have very large electron adhesion dissociative cross-sections σ [4] corresponding to the reactions $NO_2 + e \rightarrow NO + O^-$ and $N_2O + e \rightarrow N_2 + O^-$. In this case, the adhesion rate β is determined by the distribution of the electrons with respect to the energies $n(\varepsilon)$:

$$\beta = \int_0^\infty n_e(\varepsilon) v\sigma(\varepsilon) d\varepsilon,$$

and is a sharply increasing function of the field intensity. Besides dissociative adhesion, there also exists a process of triple frequency electron adhesion to the molecules of nitrogen oxide ($NO_2 + e + M \rightarrow NO_2^- + M$; $N_2O + e + M \rightarrow M + N_2O^-$), the rate of which is likewise high, but in contrast to the preceding case is a declining function of E/p.

To derive quantitative expressions which define the influence of nitrogen oxides on the energy characteristics of an electrical ionization discharge, experiments were carried out in which fixed amounts of the impurities NO_2 and N_2O were added to nitrogen of especially high purity. Oscilloscope traces of the discharge current corresponding to the various concentrations of nitrous oxide are shown in Figure 3. It can be seen that N_2O molecules possess a very high electron adhesion cross-section, which significantly exceeds the cross-section for adhesion to oxygen molecules. At a concentration of $N_2O \approx 1$ percent, the energy contribution drops off practically to zero, while the amplitude of the discharge current does not exceed the thickness of the beam on the screen of the oscilloscope. The energy contribution as a function of the concentrations of nitrous oxide and nitrogen dioxide are likewise shown in Figure 3; the energy

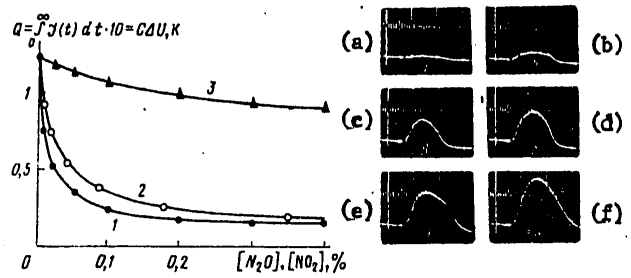

Figure 3. Characteristic oscilloscope traces of the discharge current in nitrogen with N_2O added and the curves for the integral of the discharge current as a function of the concentration of nitrous oxide (1), nitrogen dioxide (2) and oxygen (3):

a-e. 1, 0.1, 0.01, 0.005 and 0.002 % N_2O respectively;
f. Commercial grade nitrogen.

contribution due to the concentration of the oxygen impurity is also shown for the sake of comparison.

At small concentrations of electronegative impurities, the electron adhesion rate constant can be determined with a sufficient degree of accuracy from measurements of the post-pulse energy contribution, the size of which for commercial grade nitrogen is comparable to the energy contributed to the discharge during the electron current pulse. The voltage, up to which the capacitor bank is charged, is determined from the formula:

$$U_K = U_1 \exp\left(-\frac{1}{C}\int_\tau^\infty \frac{dt}{R(t)}\right), \tag{1}$$

where $U_1=U_0-\frac{1}{C}\int_0^\tau J(t)\,dt$ is the voltage corresponding to the ends of the current pulse of the electron gun; R(t) is the resistance of the decaying plasma as a function of time; C is the capacitance of the capacitor bank. The resistance of the discharge gap is determined from the formula:

$$R^{-1}(t)=\mu_e e n_e(t) S/d, \tag{2}$$

where d is the spacing between the electrodes; μ_e is the electron mobility; S is the area of the electrodes; n_e is the electron density. In order to compute the integral $\int_\tau^\infty dt/R(t)=\int_\tau^\infty \mu_e e n_e(t)\,Sd^{-1}\,dt,$ we shall employ the electron balance equation for a decaying plasma:

$$dn_e/dt=-\alpha n_e^2-\beta n_e.$$

Then:

$$\int_{\tau}^{\infty} \frac{\mu_e e n_e S}{d}\, dt = -\int_{n_{e0}}^{n_e^*} \frac{\mu_e e S}{\alpha} \frac{dn_e}{\alpha n_e + \beta} = \frac{\mu_e e S}{Cd\alpha} \ln \frac{n_{e0} + \beta/\alpha}{n_e^* + \beta/\alpha}. \qquad (3)$$

The quantity n_e^*, corresponding to the electron density at which the plasma conductivity ceases to be determined by the electron component, while the volt-ampere characteristics correspond to Thomson's formulas [5] was taken as the upper integration limit. The value of n_e^* amounts to $10^9 - 10^{10}$ cm^{-1} [6].

By taking the logarithm of both sides of equation (1) and substituting (3) in it, we obtain an expression for β in the case where $\beta/\alpha >> n_e^*$:

$$\beta = n_{e0}\alpha/[(u_1/u_h)^A - 1], \quad A = Cd\alpha/(\mu_e e S). \qquad (4)$$

The physical meaning of the coefficient A becomes understandable if the numerator and denominator of the fraction are multiplied by the electron density n_{e0}, corresponding to the moment of completion of the current pulse of the electron gun: $A = Cd\alpha n_{e0}/(e\mu_e n_{e0} S) = CR_0/\tau_{p0}$, where $\tau_{p0} = (\alpha n_{e0})^{-1}$ is the characteristic initial recombination time; R_0 is the discharge resistance at the moment of pulse completion. The coefficient A can easily vary in a wide range when performing experiments as a result of changes in the capacitance of the capacitor bank, which in the process of making the measurements was chosen so that the relative measurement error would be the least. When $\alpha n_{e0}/\beta >> 1$, the optimal value of the parameter A is determined from the formula $A_{opt} = \ln[(\alpha n_{e0}/\beta) e \tau_{\Sigma}/\tau_{p0}]$. The maximum relative measurement error using the given procedure when $A = A_{opt}$ does not exceed 12% if the voltage at the capacitor bank is measured with a precision of no worse than 2%.

The condition $\beta/\alpha >> n_e^*$ is always met with a considerable margin under actual experimental conditions. The electron adhesion rate constant is shown in Figure 1 as a function of the number of preceding electron current pulses, determined using the procedure described here. The light circles with horizontal marks above and below on this curve correspond to the values of β computed for the concentrations of the N_2O and NO_2 impurities formed in commercial grade nitrogen with the action of the electron beam. The adhesion rate constants $\langle \sigma v \rangle_{N_2O}$ and $\langle \sigma v \rangle_{NO_2}$ were determined experimentally in the processing of the oscilloscope traces of the discharge current in commercial nitrogen with monitored added amounts of the oxides; the concentration of N_2O was determined from mass spectrograms based on the intensity of the peak with a mass number of 44, while the NO_2 concentration was determined from the reduction in the oxygen in the commercial nitrogen, taking into account the formation of N_2O. It can be seen from Figure 1 that the values of β computed from the concentration of the nitrogen oxides formed in the electrical ionization discharge, within the limits of the measurement error, is related basically to the inadequate precision of the determination of the NO_2 concentration, and the values fall on the experimental curve for

$\beta(n)$. This makes it possible to conclude that the main reason for the degradation of the mixture during the operation of an EIL in a pulse periodic mode is the formation of nitrogen oxides, the molecules of which have very high electron adhesion rate constants, $\langle\sigma v\rangle \approx 10^{-10}$ cm^3/sec, which exceed the cross-section for electron adhesion to oxygen molecules by a factor of more than 100. To prevent nitrogen dioxide formation from reducing the power of the energy contribution, and correspondingly, the output radiation power, it is necessary to cool the working mixture down to a temperature at which the density of the saturating NO_2 vapors is much less than the quantity $[CO_2]\langle\sigma v\rangle_{CO_2}/\langle\sigma v\rangle_{NO_2}$. For a mixture of CO_2:N_2:He = 1:5:4 at a temperature of -70° C, the contribution of the impurity to the overall rate constant does not exceed 10 percent (without taking into account adhesion to N_2O).

We will note that cooling the mixture is necessary not only to avoid nitrogen dioxide, but also to increase the lasing efficiency and the specific power output [7]. The task of cleaning the lasing mixture of the nitrous oxide is a technically much more complex one, since N_2O has a lower boiling point (-88° C). For this reason, to completely prevent the degradation of a laser mixture during long term continuous and pulse-periodic operation of an EIL, along with cooling the gas, it is also necessary to introduce a nitrous oxide recovery system into the gas dynamic loop.

BIBLIOGRAPHY

1. N.G. Basov, I.K. Babayev, V.A. Danilychev, M.D. Mikhaylov, V.K. Orlov, V.V. Savel'yev, V.G. Son, N.V. Cheburkin, KVANTOVAYA ELEKTRONIKA [QUANTUM ELECTRONICS], 6, 772, (1979).

2. A.F. Vitshas, Ye.P. Glotov, V.A. Danilychev, V.K. Orlov, N.V. Cheburkin, V.V. Chulkov, "Preprint FIAN" ["Preprint of the Institute of Physics imeni P.N. Lebedev of the USSR Academy of Sciences"], Moscow, 1979, No 192.

3. I.A. Berezhnoy, V.A. Boyko, V.A. Danilychev, V.D. Zvorykin, V.V. Ignat'yev, I.V. Kholin, A.Yu. Chugunov, PTE [EXPERIMENTAL INSTRUMENTS AND ENGINEERING], No 5, 172, (1977).

4. R.E. Fox, J. CHEM. PHYS., 32, 285, (1960).

5. L.A. Leb, "Osnovnyye protsessy elektricheskikh razryadov v gazakh" ["The Major Electrical Discharge Processes in Gases"], Moscow-Leningrad, Gostekhizdat Publishers, 1950.

6. V.V. Aleksandrov, V.N. Koterov, A.M. Soroka, ZHURN. VYCH. MAT. I MAT. FIZ. [THE JOURNAL OF COMPUTATIONAL MATHEMATICS AND MATHEMATICAL PHYSICS], 18, 1214, (1978).

7. D.H. Douglas-Hamilton, R.M. Feinberg, R.S. Lowder, J. APPL. PHYS., 46, 3566, (1975).

8225
CSO: 1862

DYNAMICS OF FREE LASING OF SOLID-STATE LASERS

Novosibirsk DINAMIKA SVOBODNOY GENERATSII TVERDOTEL'NYKH LAZEROV in Russian 1979 signed to press 31 Oct 79 pp 2-5, 263-264

[Annotation, Foreword and Table of Contents from the book "Dinamika svobodnoy generatsii tverdotel'nykh lazerov" by K. G. Folin and A. V. Gayner, Institute of Semiconductor Physics, Siberian Department of the USSR Academy of Sciences, Izdatel'stvo "Nauka," 1,550 copies, 264 pages]

[Text] The physical factors and mechanisms which determine the time variation of the spectrum, intensity and spatial characteristics of output emission are analyzed. Because of the identity of experimental conditions for different types of lasers, a sharp difference in the dynamics of free lasing of ruby and neodymium lasers was established. The analogy between lasing and specific mechanical motion was shown theoretically, which made it possible to analyze the general properties of solutions of equations over practically the entire range of variation of laser parameters.

The book is intended for scientific workers, engineers, postgraduate students and students engaged in study and application of lasers.

Foreword

The development of modern radio-frequency amplifiers and oscillators has become possible due to the many years of careful study of the physical processes occurring in them. Similar investigations in the optical range, where the physical fundamentals of constructing devices is considerably more complex are now being continued intensively. Existing optical masers and lasers are still far from their maximum capabilities and the processes occurring in them are still far from complete understanding.

The foregoing is also true of the class of solid-state lasers which includes those based on dielectric crystals and glass activated by luminescent impurities. A. M. Prokhorov, in his foreword to the book "Fundamentals of Laser Technology" [1], notes that these lasers are the most widely used in scientific research and in technical applications since they have maximum emissivity over a wide range of pulse lengths and lasing frequency. It

should be taken into account that we are talking about lasers based on two or three of the most efficient media, while stimulated emission is achieved in more than 200 media at wavelengths from 0.31 to 3 microns. This reserve in combination with the prospects for development of the physics and chemistry of laser crystals [2] and glass indicates the high potential capabilities of solid-state lasers.

The needs of scientific and technical applications, on the one hand, and the complexity of the laser as a physical system, on the other, are the reason that investigations on the discussed topic now number in the thousands. And whereas only sections were first allocated to solid-state lasers in monographs (see, for example, [3,4]) or the entire complex of problems concerning this class of devices was considered [5], there are now papers devoted entirely to individual aspects of the problem [1, 2, 6-8].

The dynamics of free lasing of solid-state lasers is mainly investigated in the present book. The specifics of the free lasing mode are determined by a number of characteristics of a given class of devices. Specifically, the half-width of the amplification line of the active medium in a solid-state laser exceeds 10^3-10^4-fold the distance between adjacent cavity frequencies, which leads to excitation of a large number of modes. The lifetime of an atom at the upper working level is 10^4-10^5 times greater than the field relaxation time in the cavity, which is the reason for the occurrence of a prolonged oscillatory relaxation process. The process of mode interaction is complex in nature under these conditions in combination with the low rate of spatial migration of excitations and the partial dispersion of the excitation volumes of the modes in the active medium. This complexity significantly increases in the most widespread case of pulsed lasing when neither the shape nor the position of the amplification line nor the cavity configuration remains constant. Therefore, despite the fact that the main equations which describe lasing have long been known [9], it was possible until quite recently to find a solution only within the framework of simplifying assumptions (see, for example, [10]), which undoubtedly made comparison with experiment difficult. The derived solutions in the main range of laser parameter variation are weakly attenuating oscillations and the nature of lasing can be changed qualitatively due to the effect even relatively weak factors related to competition of modes or by disturbances whose effect should be carefully analyzed. The high level of technical disturbances and the high sensitivity of solid-state lasers to them severely aggravate experimental investigations.

The circumstance that there was until now no satisfactory agreement between theoretical and experimental results on some essential problems was apparently caused by the enumerated characteristics of free lasing. It is sufficient to recall, for example, the problem of the spike nature of solid-state laser emission, when the situation can be characterized by the thesis: "There are just as many opinions as there are investigators." The fact that

the experimental results found for a specific type of laser and valid only for that type were transferred to the entire class of solid-state lasers* contributed to this to a significant degree.

Thus, analysis and generalization of available results are now apparently no less timely than new investigations. Among the known publications devoted to this problem, two concern special types of lasers (traveling-wave lasers [11] and lasers with large angular divergence [7]) and only theoretical problems are considered in papers [12, 13]. The theoretical aspects of the dynamics of lasing of gas, solid-state, liquid and semiconductor lasers and also molecular and paramagnetic oscillators are analyzed mainly in the recently published monograph [10]. Practically all the known lasing modes are discussed. Naturally, with this wide range of considered problems, main attention is devoted to the principles common for all types of lasers.

New theoretical and experimental results which, in combination with known results, permit more complete characterization of free lasing of solid-state lasers, are presented in the present monograph. The conclusions outlined in the book are formulated as a result of analysis and generalization of experimental data found both by the authors with their colleagues and by other collectives. The main characteristic of constructing the theory is the use of the analogy between lasing and specific mechanical motion, which makes it possible to establish the general properties of solving multimode balance equations and to consider specifically the effect of deviations from balance approximation and some disturbances on these solutions. It is shown experimentally and theoretically that, besides technical dusturbances, there are dynamic factors which lead to non-attenuating fluctuations.

A detailed discussion of free lasing, on investigation of which the main efforts of the authors and colleagues were concentrated, is feasible with regard to the need for primary analysis and understanding of this main mode. The results obtained during investigation of it made it possible to solve problems of controlling the emission parameters of interest to practice, including those in the giant pulse operation and mode locking [14, 15]. Problems of controlling the output emission parameters are considered to the extent that they are closely related to investigation of the main principles of lasing dynamics. Successful solution of problems of this type of control is the criterion of truth for the developed concepts.

The authors are deeply grateful to Corresponding Member of the USSR Academy of Sciences V. Ye. Zuyev, who took upon himself the labor of editor-in-chief, to Corresponding Member of the USSR Academy of Sciences S. G. Rautian and Candidate of Physicomathematical Sciences G. E. Surdutovich for useful comments and also to V. S. Pivtsov and K. P. Komarov for the timely

*The authors of the given book also held this view at one time.

presented data on experimental investigation of neodymium lasers and sweep-laser theory.

V. V. Antsiferov, V. D. Ugozhayev, V. G. Gladyshev, B. M. Chernobrod, V. A. Shvets and Yu. N. Luk'yanov rendered great assistance in formulation of the text and preparation of the illustrations, for which the authors are truly grateful.

Contents Page

6521
CSO: 1862

NUCLEAR PHYSICS

COLLECTIVE ION ACCELERATION BY ELECTRON RINGS

Moscow KOLLEKTIVNOYE USKORENIYE IONOV ELEKTRONNYMI KOL'TSAMI in Russian
1979 signed to press 27 Feb 79 pp 2-4, 216

[Annotation, Foreword and Table of Contents from book "Kollektivnoye uskoreniye ionov elektronnymi kol'tsami" by V. P. Sarantsev and E. A. Perel'shteyn, Atomizdat, 1,290 copies, 216 pages]

[Text] Collective ion acceleration by electron rings is a new effective method of acceleration which was developed during the past decade. The book contains the results of theoretical and experimental investigations on collective ion acceleration. Problems of shaping the electron rings, loading them with ions and acceleration are considered. The stability of electron-ion rings in collective ion accelerators is analyzed.

The book is intended for scientific workers and postgraduate students working the field of accelerator technology and plasma physics and also for students of upper-level courses in physics specialties.

Foreword

Work has been conducted on the problem of collective ion acceleration by electron rings for the past decade in many laboratories of the world.

After the first communication at the Internation Conference on Accelerators in 1967 (United States) on the theoretical and experimental results achieved at Dubna under the supervision of V. I. Veksler, groups engaged in collective ion acceleration were created at ITEF [Institute of Theoretical and Experimental Physics] (Moscow), IYaF [Institute of Nuclear Physics] (Tomsk), Berkeley (United States), Garsching and Karlsruhe (West Germany) and other scientific centers.

The advantage of the new method is its universality--collective ion accelerators can essentially cover the entire range of energies of interest to physics investigations. Construction of collective ion accelerators is much more economically advantageous than construction of traditional accelerators. Heavy-ion collective field accelerators find the most diverse applications in industry, chemistry, biology, medicine and so on.

The intensive work of many investigators of the collective ion method is reflected in the large number of journal articles and in the proceedings of conferences and symposia. There are no monographs which generalize the numerous papers on the given topic. We feel that this book should partially fill the existing gap in survey papers on collective ion acceleration by electron rings.

In working on the book, we attempted to solve many problems. On the one hand, this book should provide an overall concept of collective ion acceleration by electron rings and, on the other hand, it should be useful to people directly involved in design of collective ion accelerators and experiments on them. Therefore, materials of a calculation-theoretical nature are included. Moreover, development of collective ion acceleration, like investigations on relativistic particle storage, stimulated careful study of the dynamics of heavy-current ring-shaped beams. The most significant aspects of this problem for the method are reflected here. Thus, we were forced to proceed toward an obviously nonuniform exposition.

We also note that the given book is far from a complete survey on collective ion acceleration. We feel that established facts are reflected in it. Many problems touched on in the book still await final solution. We hope that the book will be useful in this respect as well. In surveying the literature, we did not attempt to provide an exhaustive bibliography on the considered problem, but limited ourselves only to necessary references.

We had invaluable help when working on the book from colleagues of the Department of New Methods of Acceleration of O I Y a I [Joint Institute for Nuclear Research], specifically from V. S. Aleksandrov, Yu. I. Aleksakhin, N. Yu. Kazarinov, A. A. Popov, V. A. Preyzendorf, A. P. Sumbayev, V. S. Khabarov, V. F. Sheftsov, B. G. Shchinov, G. Shchornak and others. We express deep gratitude to all of them.

We are also very grateful to I. A. Zolina, N. A. Filippova and V. Yu. Shevtsova for the extensive work which they did in formulation of the manuscript.

Contents

6521
CSO: 1862

OPTICS AND SPECTROSCOPY

UDC 535+538.56:530.145

INTERFEROMETRIC CRITERIA FOR RADIATION FOCUSING

Moscow KVANTOVAYA ELEKTRONIKA in Russian Vol 7 No 3 (93), 1980 pp 500-505
manuscript received 8 Jul 79

[Article by M.A. Vorontsov and V.I. Shmal'gauzen, Moscow State University imeni M.V. Lomonosov]

[Text] A method is proposed to increase the operational efficiency of an adaptive focusing system for light beams, which propagate in an inhomogeneous nonlinear medium. A case of practical importance is considered, where the size of the target exceeds the size of diffraction limited light spot. The results of a numerical experiment are given, which provide evidence for the efficiency of the method.

Introduction

Adaptive optical systems in existence at the present time take the form of closed systems for the control of the phase front of light beams. The purpose of such control is the optimization of the system characteristics in presence of random external perturbations. Phase control is realized in transmitting systems of coherent optical adaptive technology (KOAT) to increase the light wave power density incident on an object, and in KOAT receiving systems to achieve the greatest angular resolution when observing through a turbulent atmosphere.

Two main classes can be ascertained among KOAT systems: phase tracked and aperture probe types [1]. The phase tracking systems are based on the use of the principle of invertibility, in accordance with which the phase distortions arising during the propagation of a light beam to an object can be compensated by introducing a certain predistortion of the phase into the initial phase profile of the transmitted wave, where this predistortion is obtained by tracking the phase of the wave propagating in the opposite direction. The principle of phase invertibility is employed only for a linear medium; under nonlinear medium conditions, it is preferable to utilize the aperture probe method.

In this method, the focusing criterion is the power of the light wave scattered by the object within the bounds of the receiving aperture (the

definition functional). It is assumed in this case that maximizing the definition functional in the receiving aperture of the object [2]. This is justified only in the case where the reflecting surface of the object has a brightly pronounced single shining spot, the area of which is less than the diameter of the incident beam [3].

A system which maximizes the definition functional has little effect if there are many highlights on the surface of the object which are similar in intensity or if the reflecting surface is homogeneously rough. Motion or rotation of the object likewise leads to a degredation of the convergence and random fluctuations in the criterion [4].

Interferometric criteria for radiation focusing, which can be used in KOAT systems are proposed in this paper. These criteria utilize information on both the phase and the amplitude of the scattered wave, and can be interpreted as a measure of the identicalness of the transmitted and scattered fields. The comparative analysis of the well known algorithm for the maximization of the definition functional and the interference algorithm performed here provides evidence of the efficiency of the utilization of the latter when KOAT systems work with objects having uniform surface roughness, i.e., in those cases where the maximization of the definition functional does not provide for efficient focusing of the radiation.

1. A Mathematical Model of an Optical System with Feedback

We shall consider an optical system with feedback which transmits the light wave energy over a certain distance z_0 in a homogeneous nonlinear medium. Let the transmitting aperture of the system produce a light beam, limited in space and time, with an initial distribution of the complex amplitude of the electrical field of:

$$E(\mathrm{r},\ 0,\ t)=E_0(\mathrm{r})e^{iu(\mathrm{r},t)};\qquad \mathrm{r}=\{x,y\};\quad 0\leqslant t\leqslant t_{\text{и}}, \tag{1}$$

where $E_0(r)$ and $u(r, t)$ are the fixed amplitude profile of the beam and its phase profile produced by the control system. The propagation of the light beam along the Z axis is described by a quasi-optical equation (for the sake of simplicity in the treatment, it is assumed that the pulse width $t_{\text{и}}$ is large, so that its delay which is related to the finiteness of the wave propagation time, can be neglected).

$$2ik\frac{\partial E}{dz}=\Delta_{\perp}E+\frac{k^2}{\varepsilon_0}\varepsilon E+RTE \tag{2}$$

and by a certain material equation LT = f(EE*). Here, $k = 2\pi/\lambda$ is the wave number; ε_0 is the dieletric permittivity of the unperturbed medium;

$\varepsilon = \varepsilon(r, z, t)$ are the perturbations of the dielectric permittivity caused by the irregular motions of the medium; R is a nonlinearity parameter; L is a certain differential operator which describes the interaction of the light wave with the medium; and f is a certain specified function of the wave intensity.

At the point $z = z_0$, the beam is scattered by the surface of the object with a scattering coefficient of $\rho(r, t)$. The boundary condition for the scattered wave, $\psi(r, z, t)$ can be written in the form:

$$\psi(r, z_0, t)=\rho(r, t)E(r,z_0,t). \tag{3}$$

For a wave $\psi(r, z, t)$ propagating in the opposite direction, in a medium with optical inhomogeneties the following equation is justified:

$$-2ik\frac{\partial\psi}{\partial z}=\Delta_\perp\psi+\frac{k^2}{\varepsilon_0}\varepsilon\psi+RT\psi, \tag{4}$$

where the function T(r, z, t) is generated with the passage of the irradiated wave. It is assumed that the power of the wave scattered by the object is low and its interaction with itself can be disregarded.

Feedback is realized in the optical system through the scattered field. The information processing device performs the current analysis of the scattered wave $\psi_0 = \psi(r, 0, t)$ within the bounds of the receiving aperture and using a certain algorithm, generates a control signal which shapes the phase profile of the transmitted wave u(r, t).

In KOAT systems which operate on the principle of phase tracking, information only on the phase of the wave which has arrived is used for the synthesis of u(r, t): $u(r, t) = -\arg\psi_0$; in this case, any functional in explicit form is not optimized.

On the other hand, in the known aperture probe systems, there is direct optimization of the image definition functional

$$J_R=\int m(r)\psi_0\psi_0^*d^2r, \tag{5}$$

where m(r) is the mask in the plane of the image. In this case, the information on the phase of the scattered field is not utilized.

2. Interferometric Focusing Criterion

We shall choose the following functional as the criterion for radiation focusing:

$$J=\left|\int m(r)E(r, 0, t)\psi(r, 0, t)d^2r\right|, \tag{6}$$

which depends both on the amplitude and on the phase of the wave scattered by the object. To investigate the conditions under which optimization of the interferometric criterion (6) leads to radiation focusing on the object, we find the criterion J considered here as a function of the field $E(r, z_0, t)$ at the object. For this, we multiply equations (2) and (4) by $m(r)\psi(r, z, t)$ and $m(r)E(r, z, t)$ respectively, subtracting the second expression from the first expression which is derived and integrate the result over r:

$$\int m \frac{\partial}{\partial z} (E\psi)\, d^2\mathbf{r} = \frac{1}{2ik} \int m (\psi \Delta_\perp E - E \Delta_\perp \psi)\, d^2\mathbf{r}.$$

We shall integrate this expression over z from 0 to z_0, and following simple tranformations of the right side, we obtain:

$$\int E_0 \psi_0 m d^2\mathbf{r} = \int m\rho E^2 (z = z_0)\, d^2\mathbf{r} + \frac{1}{2ik} \int_0^{z_0} dz \int \nabla m \mathbf{b} \psi^2 d^2\mathbf{r}, \tag{7}$$

where $E_0 = E(r, 0, t)$, while $\nabla m\mathbf{b}$ is the scalar product of the vectors $\nabla m = \{\partial m/\partial x, \partial m/\partial y\}$ and $\mathbf{b} = \{\partial(E/\psi)/\partial x, \partial(E, \psi)/\partial y)\}$. When $m(r) = 1$, i.e., in the case of an unlimited receiving aperture, expression (7) is converted to the form:

$$J = |\int \rho E^2(z_0) d^2\mathbf{r}|. \tag{8}$$

Thus, the functional J is related to the field in the plane of the object, and in this case, the form of this relationship does not depend on the inhomogeneities of the medium and remains justified taking into account nonlinearity of the kind considered here. A similar integral expression relating the definition functional J_R to the value of the field $E(r, z_0, t)$ at the object has the form:

$$J_R = \int |\rho E(z_0)|^2 m d^2\mathbf{r} + \int_0^{z_0} dz \int \nabla m \nabla \varphi |\psi|^2 d^2\mathbf{r}, \tag{9}$$

where $\phi = \phi(r, z, t) = \arg\psi(r, z, t)$. Expression (9) can be derived from equation (4) in a manner similar to the derivation of formula (7). For an unlimited receiving aperture, we have:

$$J_R = \int |\rho E(z_0)|^2 d^2\mathbf{r}. \tag{10}$$

3. A Comparative Analysis of the Integral Criteria

We shall investigate the effectiveness of applying the integral focusing criteria (5) and (6) in the operation of an aperture probe system for objects of various structures of the scattering surface. Where a single highlight is present on the object, the area of which is substantially less than

the size of the incident beam, the scattering coefficient of the surface can be represented in the form of a delta function $\rho(r, t) = \delta(r - r_0(t))$, where $r_0(t)$ the coordinate of the highlight on the surface of the object. In this case, in accordance with (8) and (10), the value of the interferometric criterion (6) agrees with definition functional (5) and is proportional to the light intensity which reaches the shining spot on the object. However, for objects with a complex scattering surface structure (the presence of several highlights which cannot be resolved by the transmitting aperture, a homogeneously rough surface), the efficiency of the algorithms for maximizing the definition and the interferometric integral differ substantially.

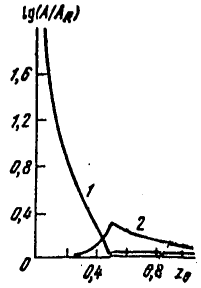

Figure 1. The ratio of the peak intensities at an object A/A_R (1) and the difference between the peak value of A and the optimal value (2) as a function of z_0.

$A = |E(0, z_0)|^2$ is the maximum value of the intensity which can be achieved by means of maximizing the interferometric integral; A_R is the same, but by means of maximizing the definition integral.

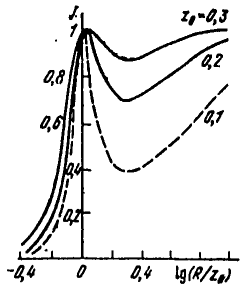

Figure 2. J as a function of R for a mirror surface.

In the following we shall consider the case of a homogeneous rough surface $|\rho(r, t)| = 1$). The definition functional (5) (when $m(r) = 1$) is a constant which does not depend on (r, t), i.e., the algorithm for maximizing the definition functional does not operate. By virtue of integral expressions (8) and (10), the nature of the relationship between the size of the focal spot and the functionals J_r should be retained in an inhomogeneous nonlinear medium. For this reason, the efficiency of such criteria for different scattering surfaces can be studied using the example of a homogeneous linear medium.

We shall consider a few very simple special cases which can be calculated analytically. We shall limit ourselves to an analysis of gaussian means: $E(x, y, 0, t)=\pi^{1/2}\exp[-(x^2+y^2)(1-i/R)/2]$. The x and y coordinates are

normalized for the initial radius of the beam a, and the radius of curvature of the initial phase front R and z are normalized for the diffraction length ka^2. We shall study the dependence of the interferometric criterion J on R for various scattering surfaces. We will note that the optimal focusing of the radiation is achieved when $R = z_0$.

A mirror surface, $\rho(r, t) = 1$. It is not complicated to show that the definition functional J_R in this case takes on the greatest value when $R = 2z_0$, which corresponds to the focusing of radiation at double the distance to the object. By using (8), one can derive an analytical expression for the interferometric criterion as a function of the radius R for an unlimited receiving aperture:

$$J=(1+d^2(R))^{-1/2}, \tag{11}$$

where $d(R)=z_0(1+1/R^2)-1/R$. . This expression has two maxima at:

$$R_\pi=[1\mp(1-4z_0^2)^{1/2}]/2z_0, \tag{12}$$

if $z_0 < 0.5$, and a single maxima when $R = 2z_0$, if $z_0 \geq 0.5$. The values of R_π here correspond to a plane phase front at the section $z = z_0$. Figure 1 illustrates the effectiveness of the utilization of the interferometric criterion in the case of an object with a mirror surface.

The curves for J(R) for various values of z_0 are shown in Figure 2. It can be seen that for successful operation of an aperture probe systems with the interferometric criterion, it is necessary to provide for preliminary focusing of the radiation, corresponding to $R < 2z_0$, which can be achieved by initially maximizing the criteria J_R.

A homogeneously rough surface. We shall consider a surface with a scattering coefficient of

$$\rho(r)=\exp\ [i\,\xi(r)], \tag{13}$$

where $\xi(r)$ is some realization of the random field ξ with a dispersion σ. The characteristic curves for J and J_R as a function of R which were obtained by means of modeling the problem on a computer for a delta-correlated field, ξ, are shown in Figure 3 ($z_0 = 0.3$).

With a comparatively small root mean square value of the roughness height ($\sigma \leq \lambda/2$), the algorithm for maximizing the interferometric criterion makes it possible in principle to realize effective focusing of the radiation. With an increase in the height of the uneven places on the surface, the efficiency of both algorithms falls off.

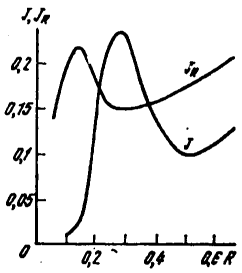

Figure 3. J as a function of J_R and R for a homogeneously rough surface (z_0 = 0.3; σ = = 0.2 λ).

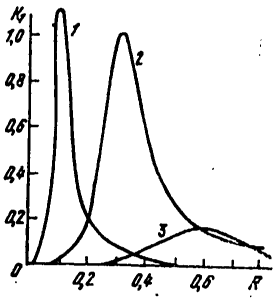

Figure 4. The criterion K_1 as a function of R for σ = 1, r_k = = 0.01 and z_0 = 0.1 (1), 0.3 (2) and 0.6 (3).

4. Statistical Focusing Criteria

The adaptive radiation focusing systems in existence at the present time are based on the assumption of the "freezability" of the inhomogeneities of the beam propagation medium and the immobility of the scattering surface of the object. The characteristic freeze time of the medium, τ_α, does not usually exceed 10^{-3} - 10^{-2} sec. However, the characteristic time during which the scattering surface of the object can be considered immobile can prove to be considerably less than τ_α (a rapidly moving or rotating object). To observe the hypothesis of freezability in this case, it is necessary to substantially increase the operational speed of the system, something which is a rather complex problem. One can take another approach and design control algorithms based on an analysis of the average characteristics of the scattered field.

The mean value of J or the mean value of J^2 can be adopted as these characteristics:

$$K=\langle J\rangle, \quad K_1=\langle J^2\rangle. \tag{14}$$

Averaging is carried out over the ensemble of realizations of the random field $\xi(r)$ of the scattering surface (13) (the mean value is measured in the experiments with respect to some rather large interval of time T).

By utilizing integral expression (8), for the case of gaussian beams propagating in a linear homogeneous medium which was treated above, the following analytical function of K(R) can be derived in the form:

$$K=\chi_4(1)/(1+d^2(R))^{1/2},$$

where $\chi_\xi(q)=\langle e^{iq\xi}\rangle$ is a characteristic function of the random field ξ; q is a real variable; the function $d(R)$ is defined in accordance with (11). Thus, the function $K(R)$ for the homogeneously rough surface of an object with the scattering coefficient of (13) agrees with the similar expression (11) for the interferometric criterion for a mirror surface (see Figure 2).

The following expression can be derived for the criterion K_1 by making use of expression (8):

$$K_1 = \iint E^2(r_1, z_0, t)E^{*2}(r_2, z_0, t)\langle\rho(r_1)\rho(r_2)\rangle d^2r_1 d^2r_2 \qquad (15)$$

In the case of a surface with a normal distribution of the random field $\xi(r)$ and a gaussian correlation function $\langle\xi(r_1)\xi(r_2)\rangle = \sigma^2\exp\{-[(x_1-x_2)^2 + (y_1-y_2)^2]/2r_k\}$ (σ is the dispersion and r_k is the correlation radius), formula (15) was used to calculate the function $k_1(R)$ on a computer. A family of such curves for $K_1(R)$ is shown in Figure 4. We will note that the maximum value of K_1 is achieved when $R = z_0$, i.e., when using this criterion it is theoretically possible to achieve the optimal focusing of the radiation on a uniformly rough surface of an object. Approximate focusing in accordance with formula (12) is possible by means of a simpler criterion K.

We will note in conclusion that the formulated criteria J, K and K_1 maximize the interferometric effect when observing a remote body. They can prove useful in studying small oscillations of bodies by interferometric methods where the bodies are observed through a distorting medium.

BIBLIOGRAPHY

1. D.Zh. Khardi, TIIER, 66, No. 6, 31 (1978).

2. R.A. Muller, A. Buffington, J. OPT. SOC. AMER., 64, 1200, (1974).

3. T.R. O'Meara, J. OPT. SOC. AMER., 67, 306, (1977).

4. S.A. Kokorowski, M.E. Pedinoff, J.E. Pearson, J. OPT. SOC. AMER., 67, 333, (1977).

8225
CSO: 1862

SUPERCONDUCTIVITY

SEMICONDUCTORS, SUPERCONDUCTORS AND PARAELECTRICS IN CRYOELECTRONICS

Moscow POLUPROVODNIKI, SVERKHPROVODNIKI I PARAELEKTRIKI V KRIOELEKTRONIKE: SVOYSTVA I PRIMENENIYE V KRIOELEKTRONNYKH INTEGRAL'NYKH SKHEMAKH I PRIBORAKH STRUKTUR NA OSNOVE KONTAKTOV POLUPROVODNIKOV, SVERKHPROVODNIKOV I PARAELEKTRIKOV [Semiconductors, Superconductors and Paraelectrics in Cryoelectronics: Properties and Application in Cryoelectronic Integrated Circuits and Devices of Structures Based on Contacts of Semiconductors, Superconductors and Paraelectrics] in Russian 1979 signed to press [not available] pp 4-9

[Annotation, foreword and table of contents from book by V.N. Alfeyev, Izdatel'stvo Sovetskoye Radio, 408 pages]

[Text] This book is devoted to the field of solid-state electronics based on the properties of a solid at cryogenic temperatures and having been given the name "integrated cryoelectronics."

Unlike V.N. Alfeyev's first book on cryoelectronics published by this press in 1966, in this book the main attention is paid to the properties of new structures based on semiconductors, superconductors and paraelectrics and to problems of the creation of equipment based on these structures and their contacts. Methods are discussed for the overall microminiaturization of cooled units of microelectronics equipment, by means of the creation of functional cryoelectronic equipment with a high degree of integration (charge-coupled devices for the IR band, multi-element amplifiers, detectors and switches), as well as highly sensitive units for equipment for the microwave and IR bands, satellite communications, space television, infrared guidance, radar, laser communications, astronomy and instrument making.

This book contains a considerable amount of original results and can be recommended for a wide range of readers, such as scientific personnel, teachers, engineers, designers and technologists, as well as as a textbook for upper-class students and graduate students.

Foreword

In recent years ever more extensive development has been given to studies on the creation of new electronic devices and complex systems based on the properties of a solid at cryogenic temperatures. Conducive to this have been not only successes in low-temperature physics and deep-freezing engineering, but also the appearance of new problems which have not been solved by other methods. Cryoelectronics embraces a wide range of problems, from the interaction of electromagnetic waves with a solid with the heavy suppression of thermal vibrations of the lattice, to methods of cooling and designing self-contained cryoelectronic devices with a cryostat case.

This monograph, being an independently completed study, at the same time continues the development of the combined utilization of the properties of different materials at low temperatures in a single structure or cooled device begun by the book "Radiotekhnika nizkikh temperatur" [Low-Temperature Radio Engineering] published by this press in 1966. Major attention is paid in this book to the properties and application of film structures based on new semiconductor materials and contacts between superconductors and semiconductors and nonlinear paraelectrics in which many phenomena have been discovered, including Josephson effects. These structures are the basis for the formation of a new trend--integrated cryoelectronics.

This book is structured on the basis of the generalization of extensive data published in domestic and foreign literature, of the author's original material, and of lectures given by him to students and graduate students in the courses "Cryogenic Microelectronics" and "Cryoelectronic Integrated Devices."

An exceptionally large role in the creation of this book, as of the monograph "Radiotekhnika nizkikh temperatur," has been played by Academician A.M. Prokhorov. The author is sincerely grateful to Academician B.M. Vul and considers it his pleasant duty to express his profound gratitude to A.I. Shokin and G.Ya. Gus'kov.

The author has been assisted for many years by his colleagues in the performance of complicated and labor intensive experimental work: Yu.V. Korenev, A.V. Ivantsov, M.I. Ugrin, T.N. Marytnik, Yu.I. Dvornikov, B.V. Tkachuk, G.V. Kuznetsov et al., whose participation is mentioned in the text. Of great benefit have been combined studies on cryoelectronic charge-coupled devices (CCD's) for the IR band and PZS's with a Schottky barrier conducted by the author with Yu.I. Shamanayev, A.I. Adrianova, A.A. Karev, O.P. Kurova and S.L. Legezo. The author is grateful to Professor Bivelogua (GDR) who kindly offered him the opportunity to become acquainted with the laboratory base for liquid neon and the investigation of paraelectrics at low temperatures, and to Professor Al'brekht for the materials of the symposium. The author is grateful to V.I. Stafeyev, V.S. Krikorova, Yu.F. Sokolov, D.P. Kolesnikov, V.V. Matveyev and B.I.

Sedunov for their valuable comments. Using this opportunity, I would like to thank the teams at MFTI [Moscow Physico-Technical Institute], KhGU [Khar'kov State University] and KGU [expansion unknown] and textbook writers M.Z. Arslanov, V.F. Ryabkov, S.V. Pertsov, K.A. Shutskiy, V.G. Fastovskiy, L.Ye. Rovinskiy, A.K. Grezin, V.S. Zinov'yev et al., who included the monograph "Radiotekhnika nizkikh temperatur" in the list of recommended textbooks, and to express the hope that this book will also go onto this list.

Appendix I was written by Ye.P. Kokin and Yu.V. Surin; sec 1.6 was written on the basis of a joint study by the author and O.G. Vendik, and secs 4.6 and 4.7 in conjunction with M.I. Ugrin. Great assistance in preparing the manuscript for publication was rendered by N.V. Alfeyev.

In the bibliography major attention is paid to domestic studies, including little-known papers delivered at various conferences. Studies by foreign authors are represented chiefly by monographs and broad surveys in which is contained an extensive bibliography on the questions touched upon.

CONTENTS

[131-8831]

8831
CSO: 1862

- END -